PHYSICAL REVIEW E VOLUME 61, NUMBER 4 APRIL 2000

Influence of through flow on binary fluid convection

P. Büchel and M. Lücke
Institut für Theoretische Physik, Universität des Saarlandes, Postfach 151150,D-66041 Saarbrücken, Germany

(Received 15 October 1999)

The influence of an externally imposed lateral Poiseuille through flow on linear, nonlinear, and transient behavior of transverse convective rolls in a horizontal layer of binary fluids heated from below is investigated. The convective roll solutions are determined numerically for realistic boundary conditions with a many-mode Galerkin expansion as well as with a finite-difference method. Bifurcation diagrams of various quantities like Nusselt number, frequency, and mixing behavior are determined as functions of heating rate and wave number for several through flow rates and Soret coupling strengths for ethanol-water parameters. The growth dynamics of small convective perturbations into different, strongly nonlinear convective states and the transition between the latter is studied also.

PACS number(s): 47.20.−k, 47.10.+g, 47.27.Te, 47.54.+r

I. INTRODUCTION

An externally imposed flow can change the spatiotemporal behavior of dissipative structures in forced nonequilibrium systems such as chemical and reaction-diffusion systems, biological problems, and the large variety of different hydrodynamic pattern forming systems [1]. One example is the stationary, toroidal Taylor vortices in the annular gap between concentric cylinders that in the presence of an axial through flow propagate in the downstream direction [2]. Here the through flow enforces a finite phase velocity on a forwards bifurcating pattern. A situation with similar bifurcation behavior occurs in a narrow rectangular convection channel filled, e.g., with water that is heated from below. Therein the convection rolls are aligned with their axes along the small side, say, in the y direction. Here a small flow through the channel in the x direction causes the transverse roll pattern to propagate downstream in the x direction [3–5]. On the other hand, in a large through flow and/or in wider channels, the through flow causes an orientation of the rolls parallel to the through flow [4].

While the investigation of heated shear flows of pure fluids has a long history—see, e.g., Ref. [6] for a review—we are not aware of similarly numerous and extensive investigations of the influence of an imposed shear flow on convective structures occurring in binary fluid mixtures such as, e.g., ethanol water [7]. This is somewhat astonishing since the bifurcation behavior and the spatiotemporal properties of the convective structures that occur close to onset in mixtures display a much larger variety than in pure fluids ([8], see also Refs. [9–17]). One observes in mixtures not only stationary roll convection—what we call for historical reasons stationary overturning convection (SOC)—as in pure fluids but also symmetry degenerate left or right traveling wave (TW) patterns. The bifurcation of both the stationary and the traveling roll structures can be either supercritical or subcritical. Thus, in both cases the transition from the quiescent heat conducting state to the convective states after crossing a critical heating rate can be either continuous, i.e., of second order or discontinuous and hysteretical, i.e., of first order depending on parameters. Furthermore, there is a wide parameter range where the primary bifurcating convective structures have the form of squares.

This richness of different convection phenomena in mixtures is due to the fact that the buoyancy, i.e., the driving force for convection is influenced by concentration variations. They are generated via the Soret effect by temperature gradients which sustain them against the action of advective mixing and diffusive homogenization. The Soret coupling between temperature and concentration field is measured by the separation ratio ψ [1]. Without Soret coupling, $\psi=0$, concentration deviations from the mean diffuse away. In this limit the concentration does not influence the longtime behavior of the mixture and one thus observes for $\psi=0$ the convective properties of a pure fluid. For $\psi\neq 0$, however, the externally imposed vertical temperature difference across the fluid layer sustains concentration variations in balance with the adverse effects of convective mixing and diffusion.

In this paper we investigate the effect of a horizontal Poiseuille through flow on stationary and traveling wave convection that appear for negative Soret coupling in ethanol-water-like mixtures. We deal here with spatially periodic, extended structures of straight transverse rolls with axes oriented perpendicular to the through flow that can be realized in narrow convection channels. This investigation provides the basis for an understanding of more complex structures occurring in long convection channels with inlet and outlet induced inhomogeneities and spatially varying amplitudes [18].

Despite the restriction to patterns with spatially homogeneous amplitudes the bifurcation behavior of these structures in the presence of through flow is surprisingly complex: The through flow lifts, first of all, the mirror symmetry degeneracy of left and right traveling waves concerning their linear as well as their nonlinear properties. Second, the through flow changes in a fundamental and spectacular way the connection and merging of the two symmetry degenerate TW solution branches with the SOC state that occurs with zero TW frequency in the absence of through flow when the finite amplitude SOC undergoes with decreasing Rayleigh number a drift instability with a left or right propagating phase.

Additional complexity comes from the fact that the SOC and TW solutions are strongly nonlinear—the advective nonlinearity in the concentration balance is typically large com-

1063-651X/2000/61(4)/3793(18)/$15.00 © 2000 The American Physical Society

pared to the diffusive linear transport—with significant hysteresis.

This paper is organized as follows: In Sec. II we describe the system and our numerical methods for investigating it. A review of the linear bifurcation properties as obtained from a linear stability analysis of the basic conductive state is presented in Sec. III. The influence of a through flow on nonlinear bifurcation properties including an investigation of the wave number dependence is contained in Sec. IV. The transient dynamics of growth, decay, and transitions between different TW types is investigated in Sec. V. The final section, Sec. VI, gives a short summary and conclusion.

II. SYSTEM

We consider a horizontal layer of a binary fluid mixture such as, e.g., alcohol-water confined between two parallel, perfectly heat conducting and impervious plates. The setup is exposed to a homogeneous gravitational field, $\mathbf{g}=-g\mathbf{e}_z$ and a temperature gradient $\Delta\underline{T}=\underline{T}_{lower}-\underline{T}_{upper}$ between the lower and upper confining boundaries. Unscaled quantities are underlined to distinguish them from the scaled ones introduced below. We investigate here convective flow patterns of straight parallel rolls as seen in many experiments. The rolls are aligned in, say, the x direction. Ignoring variations in y direction we thus describe two-dimensional (2D) convection in an x-z plane perpendicular to the roll axes.

A. Field equations

The system is described by the balance equations for mass, heat, concentration, and momentum in Oberbeck-Boussinesq approximation [19,4]

$$0=-\nabla\cdot\mathbf{u}, \tag{2.1}$$

$$\partial_t T=-\nabla\cdot\mathbf{Q}; \quad \mathbf{Q}=\mathbf{u}T-\nabla T, \tag{2.2}$$

$$\partial_t C=-\nabla\cdot\mathbf{J}; \quad \mathbf{J}=\mathbf{u}C-L\nabla(C-\psi T), \tag{2.3}$$

$$\partial_t\mathbf{u}=-\nabla(\mathbf{u}:\mathbf{u}+p-\sigma\nabla:\mathbf{u})+\mathbf{B}; \tag{2.4}$$

$$\mathbf{B}=\sigma\,\mathrm{Ra}(T+C)\mathbf{e}_z.$$

Lengths are scaled with the height d of the layer, time with the vertical thermal diffusion time d^2/κ, and the velocity field $\mathbf{u}=(u,0,w)$ with κ/d. Here, κ is the thermal diffusivity of the mixture; $T=(\underline{T}-\underline{T}_0)/\Delta\underline{T}$ denotes the deviation of the temperature from the mean temperature $\underline{T}_0$ in the fluid scaled by the temperature difference between the plates $\Delta\underline{T}$. The field $C=(\underline{C}-\underline{C}_0)\beta/(\alpha\Delta T)$ is the scaled deviation of the mass concentration $\underline{C}=\underline{\rho}_1/(\underline{\rho}_1+\underline{\rho}_2)$ of the solute from its mean $\underline{C}_0$. Here $\underline{\rho}_1$ and $\underline{\rho}_2$ are the mass density fields of the two components. For small deviations of $\underline{T}$ and $\underline{C}$ from their means the total mass density $\underline{\rho}=\underline{\rho}_1+\underline{\rho}_2$ is governed by a linear equation

$$\underline{\rho}=\underline{\rho}_0[1-\alpha(\underline{T}-\underline{T}_0)-\beta(\underline{C}-\underline{C}_0)], \tag{2.5}$$

with α, β being the thermal and solutal expansion coefficient of the fluid, respectively. For ethanol-water mixtures at room temperature α and β are positive [20].

The Lewis number L is the ratio of concentration diffusivity D and thermal diffusivity κ, and the Prandtl number σ is the ratio of momentum diffusivity ν and κ:

$$L=\frac{D}{\kappa}; \quad \sigma=\frac{\nu}{\kappa}. \tag{2.6}$$

For room temperatures (10–40 °C), the Prandtl number of ethanol-water mixtures lies between 5 and 20 [20], while for normal fluid helium it is ten or more times smaller. The Lewis number of liquid mixtures is about 0.01. In this paper we take the fluid parameters $L=0.01$ and $\sigma=10$ as representative examples for ethanol-water mixtures.

The setup is characterized by three control parameters that can be varied independently.

(i) The Rayleigh number

$$\mathrm{Ra}=\frac{\alpha g d^3}{\kappa\nu}\Delta\underline{T} \tag{2.7}$$

measures the externally imposed thermal driving due to the temperature gradient between the plates. For convenience we use the scaled Rayleigh number

$$r=\frac{\mathrm{Ra}}{\mathrm{Ra}_c^0} \tag{2.8}$$

that is reduced by the critical Rayleigh number Ra_c^0 for onset of convection in a pure fluid with the critical wave number k_c^0. The analytical values are $\mathrm{Ra}_c^0=1707.762$ and $k_c^0=3.116\,32$.

(ii) The lateral through flow driven by a lateral pressure gradient defines the Reynolds number

$$\mathrm{Re}=\langle u\rangle_z\frac{d}{\nu}, \tag{2.9}$$

where $\langle u\rangle_z$ is the vertical average of the lateral velocity field. We consider in this paper a through flow in positive x direction with positive Reynolds number.

(iii) The separation ratio

$$\psi=-\frac{\beta}{\alpha}\frac{k_T}{\underline{T}_0} \tag{2.10}$$

with the thermodiffusion ratio k_T of the mixture reflects the influence of temperature gradients on the concentration current $\mathbf{J}$. For negative separation ratios ψ, the imposed temperature gradient causes in the quiescent heat conducting state an antiparallel concentration gradient via the Soret effect. The resulting solutal contribution to the density change is opposite to the thermal contribution, thus weakens the buoyancy and stabilizes the heat conducting state. For room temperature ethanol-water mixtures, ψ values between about -0.5 and $+0.2$ can be easily realized experimentally [20]. The Dufour effect that reflects the coupling of a concentration gradient into the heat current $\mathbf{Q}$ can be discarded in binary liquid mixtures [21,22].

The buoyancy force $(\underline{\rho}-\underline{\rho}_0)\mathbf{g}$ due to density deviations from the mean is the driving mechanism for convective motion. It enters into the momentum balance (2.4) via the buoyancy term **B** which follows from Eq. (2.5) after scaling. This is the only place where density variations are retained in the Oberbeck-Boussinesq approximation. In the continuity equation (2.1), the fluid has been assumed to be incompressible, i.e., the mass density $\underline{\rho}$ is constant, and the mass current is proportional to the divergence-free velocity field $\mathbf{u}$. Taking the divergence of the Navier-Stokes equation (2.4), one gets, via the continuity equation, a Poisson equation for the pressure p. The Poisson equation substitutes the continuity equation and builds, together with Eqs. (2.2)–(2.4), a complete set of equations for the fields $\mathbf{u}$, T, C, and p.

B. Boundary conditions

The rigid, impervious, and perfectly heat conducting plates which define the horizontal boundaries of the fluid layer are located at $z=\pm\frac{1}{2}$. As boundary conditions for velocity and temperature field one obtains

$$u=w=0; \quad T=\mp\frac{1}{2} \text{ at } z=\pm\frac{1}{2}. \tag{2.11}$$

Due to the impermeability of the plates there is no concentration current through the plates, $\mathbf{J}\cdot\mathbf{e}_z=0$, or

$$\partial_z C=\psi\partial_z T \text{ at } z=\pm\frac{1}{2}. \tag{2.12}$$

Since the pressure p is determined via the Poisson equation by $\mathbf{u},T,C$, we do not need boundary conditions for it.

In the lateral direction we enforce periodic boundary conditions. All fields $F=u,w,T,C,p$ are periodic

$$F(x,z;t)=F(x+\Gamma,z;t) \tag{2.13}$$

with given periodicity Γ. For the discussion of the bifurcation scenario we will mainly focus on a lateral periodicity length of $\Gamma=\lambda=2$ which refers to a wave number of the roll patterns near the critical one but other wavelengths are explored as well. This periodicity length is also close to the values typically observed in experiments without lateral through flow when an extended bulk regime of nonlinear saturated, spatially uniform pattern amplitude exists. Note that imposing the periodicity length of one wavelength in our two-dimensional system precludes some of the instabilities of large systems, e.g., the Eckhaus instability [23] and the complex dynamical behavior found in three-dimensional experimental setups [24–26,22].

C. Conductive state

For small Ra and Re a laterally homogenous heat conducting state without convective vertical velocity is stable. In this basic state the velocity field $\mathbf{u}_{cond}=U(z)\mathbf{e}_x$ is given by the plane horizontal Poiseuille flow

$$U(z)=\sigma\,\mathrm{Re}\,P(z)=\sigma\,\mathrm{Re}\,6\left(\frac{1}{4}-z^2\right). \tag{2.14}$$

The temperature and the concentration field of the basic state are x independent and linear functions in z

$$T_{cond}=-z; \quad C_{cond}=-\psi z. \tag{2.15}$$

D. Numerical methods

The linear bifurcation properties discussed in Sec. III were obtained by solving the field equations after linearization around the conductive state with a shooting method as in Ref. [27]. Here we briefly describe the two different methods that we used to solve the full *nonlinear* hydrodynamical field equations.

On the one hand we integrated the partial differential equations (2.1)–(2.4) using a modification of the SOLA code that is based on the MAC method [28,29]. This is a finite-difference method of second order in space formulated on staggered grids for the different fields with uniform spatial resolution. An explicit first-order Euler step in time was used in the balance equations of heat (2.2) and concentration (2.3) and a second order DuFort-Frankel scheme in time was used in the momentum balance equation (2.4). The Poisson equation for the pressure field, which results from taking the divergence of Eq. (2.4), was solved iteratively using the artificial viscosity method [29]. In the finite-differences approximation of the field equations that is used in our MAC algorithm the threshold for onset of pure fluid convection [30] lies for our uniform discretization of $\Delta x=\Delta z=0.025$ at $\mathrm{Ra}^0_{stab}=1705(\pm 0.2\%)$ for $k=\pi$. So, when presenting numerical results obtained with the above discretization, we reduce Rayleigh numbers with this threshold value. As an aside we mention that the discretization in Ref. [9] was $\Delta x=\Delta z=0.05$.

In addition we also used a many-mode Galerkin approximation scheme. Our mode expansion uses the mirror glide symmetry

$$F(x,z;t)=\pm F\left(x+\frac{\lambda}{2},-z;t\right) \tag{2.16}$$

of roll patterns with spatially uniform amplitude with + for u,p and − for w,T,C [31].

The velocity field is then approximated by Chandrasekhar functions [32] that fulfill the realistic *no-slip* horizontal boundary conditions at the plates. For the vertical velocity field one obtains the representation

$$w(x,z,t)=\sum_{n=0}\sum_{m=1}[w^m_{2n+1}(t)e^{-i(2n+1)kx}+\text{c.c.}]C^m(z) + \sum_{n=0}\sum_{m=0}[w^m_{2n}(t)e^{-2inkx}+\text{c.c.}]S^m(z). \tag{2.17a}$$

Lateral and vertical velocity fields are coupled via the continuity equation. For TW patterns there exists also a weak, x independent meanflow in the lateral direction that is also expanded in Chandrasekhar functions. The deviation of the temperature field from the conductive profile, $\theta=T-T_{cond}$, is expanded in trigonometric series

$$\theta(x,z,t)=\sum_{n=0}\sum_{m=1}[\theta^{2m}_{2n}(t)e^{-2inkx}+\text{c.c.}]\sqrt{2}\sin(2m\pi z) + \sum_{n=0}\sum_{m=0}[\theta^{2m+1}_{2n+1}(t)e^{-i(2n+1)kx}+\text{c.c.}] \times\sqrt{2}\cos[(2m+1)\pi z]. \tag{2.17b}$$

Within the Galerkin method the impermeability condition (2.12) is conveniently ensured by using the combined field $\zeta=(C-C_{cond})-\psi\theta$ instead of the concentration field. This auxiliary field obeys the boundary conditions $\partial_z\zeta=0$ at $z=\pm\frac{1}{2}$. Thus, it is expanded as

$$\begin{aligned}\zeta(x,z,t)=&\sum_{n=0}\sum_{m=0}[\zeta_{2n}^{2m+1}(t)e^{-2inkx}+\text{c.c.}]\\&\times\sqrt{2}\sin[(2m+1)\pi z]\\&+\sum_{n=0}\sum_{m=0}[\zeta_{2n+1}^{2m}(t)e^{-i(2n+1)kx}+\text{c.c.}]\\&\times\sqrt{2-\delta_{m,0}}\cos(2m\pi z).\end{aligned}\tag{2.17c}$$

The expansion of the velocity field in the x and z directions was truncated at $n_{\mathbf{u}}=m_{\mathbf{u}}=3$. Also the meanflow contained three modes in z. However, the θ as well as the ζ field were expanded up to $n_{\theta,\zeta}=m_{\theta,\zeta}=19$ to ensure a sufficient resolution of concentration boundary layers.

Projecting the field equations for w, θ, and ζ onto the bases of the mode expansion (2.17) yields coupled ordinary differential equations for the mode amplitudes $w_n^m(t)$, $\theta_n^m(t)$, and $\zeta_n^m(t)$. For SOC solutions all mode amplitudes are constant in time and can be chosen to be real. In a relaxed TW, however, with constant oscillation frequency ω and phase velocity $v_{ph}=\omega/k$ the complex mode amplitude of a lateral Fourier mode, e^{-inkx}, oscillates with frequency $n\omega$. To solve the coupled equations for the mode amplitudes we use a Newton-Raphson technique with backtracking. We iteratively adjust the mode amplitudes and the oscillation frequency of a TW for fixed control and fluid parameters starting from given initial values. To follow the bifurcation branches it was sometimes more convenient to iteratively adjust the Rayleigh number r for given convective amplitude w_1^1.

E. Order parameters

To characterize the convective solutions we use different order parameters:

(i) The Nusselt number

$$N=\frac{1}{\Gamma}\int_0^\Gamma dxQ_z\tag{2.18}$$

is the total vertical heat current through the fluid layer, $\int_0^\Gamma dxQ_z$, reduced by the conductive part, $\int_0^\Gamma dxQ_{cond}=\Gamma$. In our scaling, $Q_{cond}=1$. The reduced vertical heat current carried by convection alone, $N-1$, is a measure of the convective flow intensity.

(ii) To characterize the concentration field in the nonlinear convective states we use the mixing parameter

$$M=\sqrt{\langle C^2\rangle/\langle C_{cond}^2\rangle},\tag{2.19}$$

which measures the size of concentration variations: M is the variance of the concentration field reduced by its value in the conductive state. Here, brackets imply a spatial average over the whole fluid volume. In a perfectly mixed mixture where all concentration deviations C from the mean vanish, M would be zero. On the other hand, in the conductive state with Soret-induced concentration gradient, M is defined to be 1.

(iii) TW states are characterized by their oscillation frequency ω which, by the way, is very closely related to the size of M [33].

III. LINEAR BIFURCATION PROPERTIES

In this section we briefly review the influence of through flow on linear bifurcation properties of different convective patterns [27]. We focus here our interest on small Reynolds numbers. For sufficiently large Re, the lowest relevant bifurcation threshold of binary mixtures with any ψ asymptotically approaches the critical Rayleigh number of pure fluid convection [27] since in this limit the externally imposed shear flow effectively eliminates the Soret-induced coupling effects between the convective concentration field and the other fields by suppressing vertical convective transport of Soret driven concentration perturbations.

A. Stability analysis of the basic state

For a linear stability analysis of the basic state one considers the field equations

$$\begin{aligned}(\partial_t-\sigma\nabla^2)\nabla^2w+(U\nabla^2-\partial_z^2U)\partial_xw\\=\text{Ra}\,\sigma(\partial_x^2+\partial_y^2)[(1+\psi)\theta+\zeta],\end{aligned}\tag{3.1a}$$

$$(\partial_t-\nabla^2+U\partial_x)\theta=w,\tag{3.1b}$$

$$(\partial_t-L\nabla^2+U\partial_x)\zeta=-\psi\nabla^2\theta,\tag{3.1c}$$

which are linearized in the small deviations $w,\theta,$ and ζ from the conductive state. The fields are laterally Fourier decomposed

$$\Phi(\mathbf{r},t)=\hat{\Phi}(z)e^{i(k_xx+k_yy)}e^{st}\tag{3.2}$$

with a complex characteristic exponent

$$s=\text{Re}\,s+i\,\text{Im}\,s=\gamma-i\omega\tag{3.3}$$

and complex z-dependent amplitudes of the perturbations

$$\hat{\Phi}=(\hat{w},\hat{\theta},\hat{\zeta}).\tag{3.4}$$

Inserting the ansatz (3.2) into the field equations (3.1) one obtains a 3×3 system of ordinary differential equations for $\hat{\Phi}(z)$ that are nonautonomous in the presence of through flow [27]. Due to the boundary conditions the eigenvalue spectrum is discrete. We are interested in the three characteristic exponents $s_j(j=1,2,3)$ whose temporal growth rates γ_j are closest to zero and whose eigenfunctions $\hat{\Phi}_j(z)$ have no nodes other than those at the horizontal boundaries.

The horizontal wave vector $\mathbf{k}$ of the perturbation (3.2) and the through flow Reynolds number Re enter into Eq. (3.1) only as $k^2=k_x^2+k_y^2$ and $k_x\,\text{Re}$. Therefore, one can invoke the Squire transformation [34]

$$f(k_x^2+k_y^2,k_x\,\text{Re})=f(k^2,k\,\text{Re}\cos\varphi)\tag{3.5}$$

with φ denoting the inclination angle of the roll axes compared to the direction of the imposed through flow. For a complete stability analysis one has to consider only perturbations with wave vectors $\mathbf{k}=k_x\mathbf{e}_x$ which are parallel or antiparallel to the through flow direction. The linear behavior of other types of rolls with $\varphi\neq 0,\pi$, e.g., longitudinal ones, can be extracted with Eq. (3.5) by rescaling the through flow Reynolds number with $\cos\varphi$ [27]. In the absence of through flow, Re$=0$, the Squire transformation (3.5) reflects the horizontal rotational symmetry of the system.

B. Absence of through flow

The stability properties of the conductive state against infinitesimal convective perturbations in the absence of through flow have been discussed in detail in the literature [35,36,38,37]. For ψ above (below) the tricritical value $\psi^t_{SOC}=-O(10^{-7})$ [37], the SOC bifurcation is forwards (backwards). However, below $\psi^{\infty}_{SOC}=-L/(1+L)$ [39,40] where the stationary threshold r_{stat} diverges, the lower SOC solution branch is disconnected from the conductive solution for positive r [41]. In addition, there exists for strong stabilizing Soret coupling a Hopf bifurcation threshold at r_{osc} where symmetry-degenerated left and right traveling wave solutions branch out of the conductive state. The Hopf frequency, ω_H, varies as $\omega_H^2\approx -449\psi/(1+\psi+1/\sigma)$ [42,43]. For ψ above (below) the tricritical value $\psi^t_{TW}=-O(10^{-4})$ [37,44] the TW bifurcation is forwards (backwards). The bifurcation thresholds r_{stat} and r_{osc} become equal at the codimension-two value $\psi_{CTP}=-O(10^{-5})$ with slightly different critical wave numbers and a small Hopf frequency. For a more detailed discussion of the codimension-two point see, e.g., Refs. [35–38,45,46].

C. Notation

Instead of numbering the three different bifurcation thresholds and bifurcating convective solutions of the 3×3 eigenvalue problem (3.1) in the presence of through flow, Re>0, we use henceforth superscripts *S*, *U*, *D*. They identify the behavior of critical perturbations, $e^{i(k_c x-\omega_c t)}$, in the limit Re$\to 0$. Eigenvalues for which $\omega_c(\mathrm{Re}\to 0)=0$ are marked by *S*, since these perturbations are stationary for Re$=0$. Eigenvalues for which $\omega_c(\mathrm{Re}\to 0)$ is positive (negative) carry the superscript *D* (*U*), since they characterize perturbations which propagate in downstream (upstream) direction for Re $\to 0$. Thus, the cases *S* (‘‘stationary’’), *D* (‘‘downstream’’), and *U* (‘‘upstream’’) characterize the perturbations and with it the bifurcating nonlinear solutions in the limit Re$\to 0$. For convenience we use this notation also in the absence of through flow, Re$=0$. Then $D(U)$ identifies a TW where the phase is propagating to the right (left) with frequency $\omega^D>0$ ($\omega^U<0$).

Finally we should like to draw attention to the fact that we distinguish the propagation direction of different TW's by their frequency not by their wave vector—we only consider positive $k_x=k$ in this work.

D. Through-flow-induced symmetry breaking of the oscillatory instability

We briefly review in this subsection the critical properties of a binary mixture such as ethanol water with $\psi=-0.25$ as a representative case for moderately negative Soret couplings. In the absence of through flow, the threshold of stationary convection has already disappeared since $\psi>\psi^{\infty}_{SOC}=-L/(L+1)$. There exists only the Hopf bifurcation threshold at $r_{osc}=1.3348$ for symmetry degenerate left or right propagating TW's with the critical Hopf frequency $\omega_H=11.2125$. Finite through flow breaks the symmetry of the two TW patterns and different, up- and downstream propagating TW's bifurcate out of the conductive state. They will be referred to as TWU (traveling wave upstream) and TWD (traveling wave downstream).

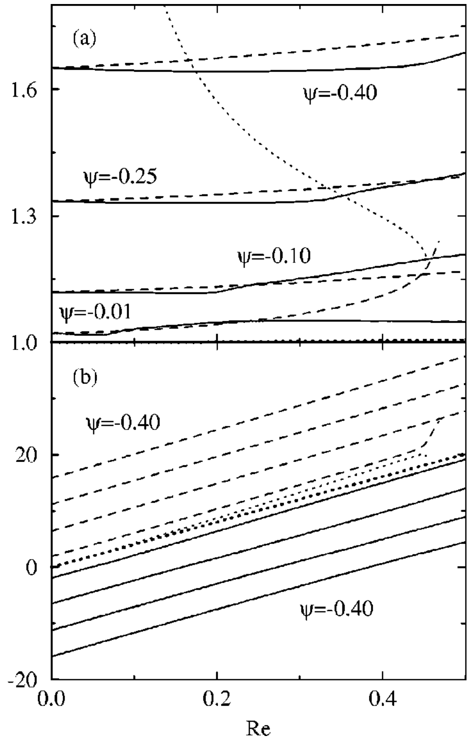

FIG. 1. Through flow dependence of critical properties for negative Soret coupling ψ. In (a) we show the bifurcation thresholds r_c^U, r_c^D, and r_c^S and in (b) the critical frequencies ω_c^U, ω_c^D, and ω_c^S for the three propagating wave solutions *U* (full lines), *D* (dashed lines), and *S* (thin dotted lines). Thick dotted lines refer to the pure fluid, $\psi=0$. Parameters are $L=0.01, \sigma=10$.

The relative difference between the critical wave numbers k_c^D and k_c^U of the *D* and *U* waves, repectively, is not more than a few percent for the mixtures and Reynolds numbers considered here. The critical frequencies ω_c^D and ω_c^U are practically linear functions of Re. They start at zero through flow with the Hopf values ω_H and $-\omega_H$, respectively, and they can be very well approximated by the first-order result of a low-Re expansion [27]

$$\omega_c^{D,U}=\pm\omega_H+41.9\,\mathrm{Re}. \tag{3.6}$$

The rate of change $\partial\omega_c/\partial\mathrm{Re}\approx 41.9$ also holds for other separation ratios [27] including the pure fluid case [47] as can be seen in Fig. 1(b).

Note that for $\mathrm{Re}\geqslant\omega_H/41.9$ both critical frequencies, ω_c^D and ω_c^U, as well as the phase velocities $v_{ph}^{D,U}=\omega_c^{D,U}/k_c^{D,U}$ are positive. Then both critical waves propagate in through flow direction in the laboratory frame. However, v_{ph}^{U} is always smaller—by about $2\omega_H/k_c(\mathrm{Re}=0)$—than v_{ph}^{D}. Only for $\mathrm{Re}\leqslant\omega_H/41.9$ the phase velocity, v_{ph}^{U}, is negative and opposite to the through flow. So, the wording ''upstream traveling waves'' does not necessarily imply that the phase velocity of such a TW is negative in the laboratory frame. It would be negative in a frame moving in through flow direction with a conveniently defined mean lateral velocity such as, e.g., $\overline{v}=\frac{1}{2}(v_{ph}^{U}+v_{ph}^{D})$.

E. Bifurcation thresholds at negative ψ

Here we discuss the bifurcation thresholds r_c^U (full lines), r_c^D (dashed lines), and r_c^S (dotted lines) as functions of Re for a few characteristic negative Soret couplings as shown in Fig. 1(a).

1. $r_c^U(\mathrm{Re},\psi)$

With increasing through flow rates r_c^U [full lines in Fig. 1(a)] decreases for small Re, develops a minimum close to where ω_c^U goes through zero, steeply increases thereafter, and finally flattens asymptotically for any Soret coupling ψ towards the Re-dependent pure fluid stability boundary $r_c(\mathrm{Re},\psi=0)$ at large Re. The flattening of r_c^U can be seen in Fig. 1(a) only for the weaker Soret coupling $\psi=-0.01$. With increasing Soret strength the flattening of r_c^U towards $r_c(\mathrm{Re},\psi=0)$ shifts to larger and larger Re [27] outside the plot range of Fig. 1. Thus a sufficiently large through flow eliminates the Soret induced coupling effects between the concentration field on one side and the temperature and velocity field on the other side. For small ψ, e.g., at $\psi=-0.001$, the stability boundary r_c^U lies always below r_c^D while for larger $|\psi|$ there are two intersections of the curves r_c^U and r_c^U with $r_c^D\leqslant r_c^U$ in between [27]. Note, however, that the bicritical TWU and TWD perturbations cannot be superimposed linearly to a standing wave, since their wave numbers $k_c^U\neq k_c^D$ differ, and furthermore $\omega_c^U\neq-\omega_c^D$. So, in the Re-interval between the intersections of r_c^U and r_c^D downstream propagating convection waves grow first while outside this interval at small Re and large Re TWU convection bifurcates first out of the conductive state.

2. $r_c^D(\mathrm{Re},\psi)$

The bifurcation threshold r_c^D [dashed lines in Fig. 1(a)] always increases monotonically with Re. The initial slope $\partial r_c^D/\partial\,\mathrm{Re}$ increases somewhat with decreasing $|\psi|$. For $\psi=-0.01$ the stability curves r_c^D and r_c^S collide in the Re range displayed in Fig. 1. For higher through flow rates there opens up a wave number gap where neither TWD nor TWS perturbations can grow [27,48,18].

3. $r_c^S(\mathrm{Re},\psi)$

For pure fluid convection, $\psi=0$, the bifurcation threshold $r_c(\mathrm{Re},\psi=0)$ [thick, dotted curve in Fig. 1(a)] slightly increases with growing Re [6]. In the absence of through flow, r_c^S rapidly increases with $|\psi|$ and diverges at $\psi_{SOC}^{\infty}=-L/(L+1)$. Beyond this Soret coupling the solution branch of stationary nonlinear convection is disconnected from the basic state as $r_c^S(\mathrm{Re}=0,\psi\leqslant\psi_{SOC}^{\infty})=\infty$. A small but finite through flow, however, moves the threshold r_c^S down to finite values: The dotted curve for r_c^S of Fig. 1(a) for $\psi=-0.01<\psi_{SOC}^{\infty}$ shows (i) that $r_c^S=\infty$ below a finite $\mathrm{Re}_\infty\simeq0.019$, (ii) that r_c^S is finite for $\mathrm{Re}>\mathrm{Re}_\infty$, and (iii) that r_c^S steeply drops down for $\mathrm{Re}>\mathrm{Re}_\infty$ [27]. The Reynolds number Re_∞ where r_c^S diverges grows with increasing $|\psi|$—a stronger Soret coupling requires a larger through flow to move the bifurcation threshold r_c^S from infinity to a finite value.

IV. NONLINEAR BIFURCATION BEHAVIOR

In this section we discuss the influence of an externally imposed lateral through flow on the nonlinear bifurcation behavior of tranverse convective rolls of a given lateral periodicity length $\Gamma=\lambda=2$ in mixtures with buoyancy-reducing negative Soret effect. The through flow causes stationary patterns to propagate and furthermore lifts the symmetry degeneracy between left and right propagating TW's at $\mathrm{Re}=0$. The right (left) propagating wave with positive (negative) frequency at $\mathrm{Re}=0$ becomes a TWD (TWU) in the presence of through flow. Not only the onset Rayleigh number and initial frequency of TWD and TWU differ but more importantly the symmetry degenerate zero-frequency merging of the two TW's with the SOC occurring at $\mathrm{Re}=0$ is dramatically changed by the through flow. To elucidate the influence of a through flow we first review a typical bifurcation diagram for $\psi=-0.25$ at $\mathrm{Re}=0$ determined with the finite-differences MAC algorithm with $\Delta x=\Delta z=0.025$. In the second part of this section we discuss the variation of bifurcation behavior and field structure for different Soret coupling strengths with increasing through flow rates. Finally the wave number dependence of the order parameters is presented. For finite through flow rates all order parameters presented in Figs. 2–8 are determined with the many-mode Galerkin method with a mode truncation of $n_{\theta,\zeta}=m_{\theta,\zeta}=19$ and $n_{\mathbf{u}}=m_{\mathbf{u}}=3$ for the velocity field as well as for the mean-flow.

A. Bifurcation behavior in the absence of through flow

In the left column of Fig. 2 we show the r dependence of mixing parameter M, frequency ω, and Nusselt number $N-1$ of the convective states with spatially uniform amplitude and wavelength $\lambda=2$ in a mixture with parameters $\mathrm{Re}=0$, $L=0.01$, $\sigma=10$, $\psi=-0.25$ [9,10]. These diagrams display in a representative way the subcritical bifurcation topology that is typical for sufficently negative Soret coupling ψ. The dotted line in Fig. 2(c) gives for comparison the Nusselt number of SOC in a pure fluid, $\psi=0$.

The conductive state becomes unstable at $r_{osc}=1.3348$. Just above r_{osc} the system does not saturate in a state with small convective amplitude as in a pure fluid. Here two strongly nonlinear, symmetry degenerate TW's of *large* amplitude are stable above threshold. For simplicity we refer in this section to right propagating waves with positive frequency only. But their mirror images, the left propagating waves with negative frequency, are meant in an analogous way as well.

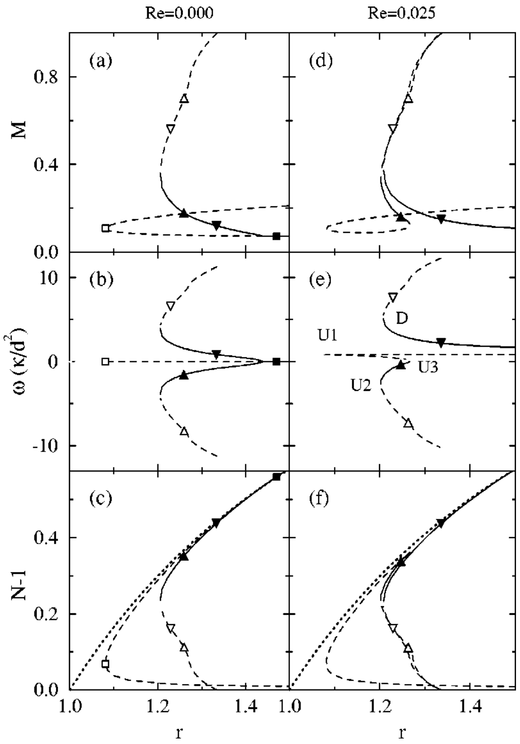

FIG. 2. Influence of lateral through flow on bifurcation properties of transverse roll convection. Shown are from top to bottom mixing number *M*, frequency ω, and Nusselt number $N-1$ versus reduced Rayleigh number *r* in the absence of through flow, $\mathrm{Re}=0$ (left column), and in the presence of a small through flow, $\mathrm{Re}=0.025$ (right column). Full (dashed) lines with filled (open) symbols denote stable (unstable) solutions. Right propagating TW's at $\mathrm{Re}=0$ and TWD's at $\mathrm{Re}=0.025$ are shown by lines with downwards pointing triangles. Left propagating TW's at $\mathrm{Re}=0$ and TWU's at $\mathrm{Re}=0.025$ are shown by lines with upwards pointing triangles. The SOC solution that exists only at $\mathrm{Re}=0$ is shown in the left column by lines with squares. TWD and TWU saddles in finite through flow are identified by *D*, *U*1, *U*2, *U*3, respectively, in (e). Dotted lines in (c) and (f) refer to pure fluid convection, $\psi=0$. Parameters are $L=0.01$, $\sigma=10$, $\psi=-0.25$, $k=\pi$.

The nonlinear TW state at r_{osc} has a frequency of only about $\frac{1}{10}\omega_H$. When reducing the drive *r* the TW frequency increases up to about $\frac{1}{3}\omega_H$ at the saddle $r_S^{TW}\simeq 1.206$. Below this saddle the system undergoes a transition to the conductive state. The reason for the associated discontinuous onset of convection is a nonlinear feedback: For $\psi<0$, the Soret-induced conductive concentration distribution weakens the buoyancy. Convection, on the other hand, redistributes the alcohol more evenly, thereby reducing the adverse Soret effect and thus increasing the buoyancy much more strongly than the flattening of the vertical temperature profile in the bulk decreases the buoyancy. The increased buoyancy in turn strengthens convection, which again amplifies the buoyancy.

With increasing *r* the TW frequency decreases to zero, until there is a continuous transition at r^* to SOC. For larger *r* one obtains stable SOC states. The transition at $r^*\simeq 1.427$ between the TW branch [solid lines with upwards (downwards) pointing, filled triangles for left (right) traveling waves in Fig. 2] and the SOC branch (solid lines with filled squares in Fig. 2) is smooth and nonhysteretic. Viewed from the stable SOC branch above r^*, we have with decreasing *r* a drift instability associated with a symmetry-breaking forward bifurcation to left or right traveling waves.

The unstable *upper* SOC branch with the larger Nusselt number [dashed line with open square in Fig. 2(c)] can be stabilized below r^* down to the SOC saddle at $r_S^{SOC}\simeq 1.078$ by enforcing a pinning of the phase by imposing the condition $u(x,z;t)=0$ at $x=0,\Gamma$. So, in our short system of length $\Gamma=2$ the roll pair cannot travel. In somewhat longer systems, however, this pinning is not sufficient to prevent TW's in the bulk, as has been seen in simulations of a system of length $\Gamma=10$ [49] and similarly in experiments [50–53]. Furthermore, we have stabilized also the unstable *lower* bifurcation branches of SOC and TW solutions [dashed lines with open symbols in Fig. 2(c)] with smaller Nusselt numbers by using an adaptive control mechanism in the MAC simulations [33].

The Nusselt numbers of TW and SOC states typically lie just below the values for a pure fluid [dotted line in Fig. 2(c)]. Only near the saddles there are stronger deviations. That our SOC and TW states are closer to SOC states in a pure fluid than to the conductive state of the mixture is reflected also in the mixing parameter *M* [Fig. 2(a)] of the concentration field. Convective mixing of stable SOC patterns dramatically reduces concentration variations to $M\simeq 0.1$ with a slight increase at the saddle. The convective homogeneization of concentration, measured in terms of *M*, is more efficient by a factor of 3.5 in SOC states than in a TW at its saddle.

Note that the curve of M_{TW} [lines with triangles in Fig. 2(a)] has the same form as that of ω versus *r* in Fig. 2(b). In fact, TW frequency and TW concentration variations are closely linked together—$M_{TW}\simeq\omega/\omega_H$ for not too small ω [33].

B. Phase dynamics near the drift instability

In the absence of through flow the transition from SOC at $r\geqslant r^*$ to TW states at $r<r^*$ is a drift instability. To elucidate and to understand how the through flow influences this transition we also used an extension of a few-mode Galerkin model [54] for SOC and TW convection to the case of through flow. From this model we derive coupled equations for the phases of the relevant modes. These phase equations allow in particular to explain the change of the bifurcation diagrams of ω versus *r* close to r^* from the pitchfork topology in Fig. 2(b) to a shifted, imperfect bifurcation in Fig. 2(e) to be a result of the through flow perturbation: It breaks the left-right symmetry and in addition causes an upward shift of the phase velocities, i.e., the frequencies of the two traveling waves.

The few-mode Galerkin model [54] is based on the field truncation

$$w(x,z,t)=[w_{11}(t)e^{-ikx}+\mathrm{c.c.}]\cos^2(\pi z), \qquad (4.1)$$

$$T(x,z;t)=-z+T_{02}(t)\sqrt{2}\sin(2\pi z)+[T_{11}(t)e^{-ikx}+\mathrm{c.c.}]\sqrt{2}\cos(\pi z), \qquad (4.2)$$

$$C(x,z,t)=-\psi(\{1+2\pi\sqrt{2}[c_{02}(t)-2c_{04}(t)]\}z$$
$$+c_{02}(t)\sqrt{2}\sin 2\pi z+c_{04}(t)\sqrt{2}\sin(4\pi z)$$
$$+[c_{10}(t)e^{-ikx}+\text{c.c.}]\sqrt{2}$$
$$+[c_{12}(t)e^{-ikx}+\text{c.c.}]$$
$$\times\sqrt{2}\cos(2\pi z)). \tag{4.3}$$

This field representation was shown to describe the bifurcation properties of TW and SOC rolls at $\mathrm{Re}=0$ quite well [54]. For $k=\pi$, we write the complex modes $w_{11},T_{11},c_{10},c_{12}$ in polar form

$$\frac{8}{5\pi^2}w_{11}=Xe^{i\phi_X},\quad \frac{6\pi\sqrt{2}}{5}rT_{11}=Ye^{i\phi_Y}$$

$$\frac{32\sqrt{2}}{5}rc_{10}=U_1e^{i\phi_{U_1}},\quad \frac{32\sqrt{2}}{5}rc_{12}=U_2e^{i\phi_{U_2}} \tag{4.4a}$$

with the same scaling coefficients as in Ref. [54]. The modes

$$\frac{6\pi\sqrt{2}}{5}rT_{02}=Z,\quad \frac{256\sqrt{2}}{15\pi}rc_{02}=V_1,\quad \frac{256\sqrt{2}}{5\pi}rc_{04}V_2 \tag{4.4b}$$

are real. For SOC patterns the fields have common fixed phases, $\phi_X=\phi_Y=\phi_{U_1}=\phi_{U_2}$, and the amplitudes X,Y,Z,U_1,U_2,V_1,V_2 are constant in time. Also in a TW the field amplitudes are constant in time. However, the four phases increase in time with a common rate $\partial_t\phi=\omega$ given by the TW frequency in such a way that the phase differences

$$\alpha=\phi_X-\phi_Y,\quad \beta=\phi_X-\phi_{U_1},\quad \gamma=\phi_X-\phi_{U_2} \tag{4.5}$$

are constant in time.

Inserting the mode representations (4.4) into the model equations of Ref. [54] one obtains coupled equations for the amplitudes X,Y,Z,U_1,U_2,V_1,V_2 and the phases $\phi_X,\phi_Y,\phi_{U_1},\phi_{U_2}$. Rewriting the latter in terms of $\varphi=\phi_X$ and the phase differences (4.5) one finally has

$$\frac{\tau}{\tilde{\sigma}}\dot{\varphi}=-\frac{Y}{X}\sin\alpha+a\psi\left[\frac{U_1}{X}\sin\beta+\frac{U_2}{2X}\sin\gamma\right]-\frac{b}{\tilde{\sigma}}\,\mathrm{Re}, \tag{4.6a}$$

$$\tau\dot{\alpha}=\tau\dot{\varphi}-(r-Z)\frac{X}{Y}\sin\alpha+c\,\mathrm{Re}, \tag{4.6b}$$

$$\tau\dot{\beta}=\tau\dot{\varphi}+\left[r+\frac{5a}{2}\left(V_1-\frac{4}{9}V_2\right)\right]\frac{X}{U_1}\sin\beta+\left(d+e\frac{U_2}{U_1}\right)\mathrm{Re}, \tag{4.6c}$$

$$\tau\dot{\gamma}=\tau\dot{\varphi}+\left[r+\frac{10a}{3}\left(V_1-\frac{1}{6}V_2\right)\right]\frac{X}{U_2}\sin\gamma+\left(f+e\frac{U_1}{U_2}\right)\mathrm{Re} \tag{4.6d}$$

with $\tilde{\sigma}=\frac{27}{14}\sigma$, $\tau=1/2\pi^2$, $a=9\pi^2/128$. The terms in front of the Reynolds number Re come from the extension [18] to finite through flow. Their effect will be discussed further below.

1. Absence of through flow

We consider first $\mathrm{Re}=0$. One first of all sees that for phase differences $\alpha=\beta=\gamma\equiv 0$ one has $\dot{\varphi}=0$, i.e., the SOC state. Traveling waves can exist only for nonvanishing phase differences. In the immediate vicinity of the SOC-TW transition the phase differences are small and one can expand the equations for mode amplitudes and phase differences in lowest order of α,β,γ. Then, the mode amplitudes are those of the SOC states, i.e., constant, and Eqs. (4.6) describe for $\mathrm{Re}=0$ a drift instability in a way that resembles the amplitude equation description of a drift instability by Fauve *et al.* [55]. Here, in our case the SOC fixed point of the few-mode Galerkin model loses stability at r^* and immediately below r^* a drifting pattern with finite α,β,γ and finite $\omega^2=\dot{\varphi}^2\propto(r^*-r)$ is stable [54]. Thus, the curve ω versus r undergoes a pitchfork bifurcation at r^*. However, due to the smallness of the Lewis number the phase differences β and γ grow rapidly with ω. Already for very small frequencies β and γ reach values around $\pi/2$, whereas α remains small.

2. Through-flow-induced imperfection

Incorporating the through flow into the field equations give rise to the Re terms in Eqs. (4.6) with constant coefficients b,c,d,e,f. With *free-slip* boundary conditions for the velocity field at the plates one obtains $b=c=d=f$, and the coupling coefficient e between U_1 and U_2 vanishes due to the orthogonality relation of the mode ansatz for the concentration field. In this free-slip case, the *z*-independent through flow leads only to a frequency shift which is proportional to the through flow rate Re. But otherwise the bifurcation scenario remains unchanged since the free-slip plug flow can be compensated by a Galilei transformation.

Enforcing realistic *no-slip* boundary conditions for the velocity field at the plates, the Poiseuille profile $P(z)$ leads to different values of *b*, *c*, *d*, and *f*, and in addition there exists an off-diagonal coupling, $e\neq 0$, between U_1 and U_2. Therefore the effect of through flow cannot be scaled out of the equations via a Galilei transformation, and one observes in addition to a frequency shift an imperfection of the frequency bifurcation. Both effects can be qualitatively described as resulting from a shifted, imperfect pitchfork bifurcation

$$0=(r^\star-r)(\omega-\alpha_1\,\mathrm{Re})-\alpha_2(\omega-\alpha_1\,\mathrm{Re})^3+\alpha_3\,\mathrm{Re}. \tag{4.7}$$

C. Bifurcation behavior in the presence of through flow

Here we discuss how the through flow changes the $\mathrm{Re}=0$ bifurcation topology globally. To that end we first present in the right column of Fig. 2 the influence of a *small* through flow, $\mathrm{Re}=0.025$, on the bifurcation diagrams for $\psi=-0.25$. In Sec. III E we have investigated the linear stability thresholds r_c^S, r_c^D, and r_c^U for TWS, TWD, and TWU perturbations, respectively. Since in the presence of through flow the bifurcation branches starting from either r_c^D or r_c^U are connected at large r with r_c^S for vanishing convective amplitude (or extend with small amplitude to ∞ when r_c^S is infinite), we will discard the superscript S to guarantee that there is no ambiguity and use only the superscripts D and U.

1. TWD's

A through flow causes SOC patterns to propagate downstream. Thus the through flow transforms the SOC solution branch and with it the former SOC-TW transition: the branch of right propagating TW's with positive frequency joins continuously with the branch of downstream propagating states that evolves with increasing Re out of the former stable SOC branch for $r>r^*$. In accordance to the linear results we call this branch the TWD branch. It is marked by downwards pointing triangles in the right-hand column of Fig. 2.

The TWD solution branch for M, ω, and $N-1$ contains one saddle [marked by the letter D in the $\omega-r$ bifurcation diagram of Fig. 2(e)]. There the TWD solution being unstable at onset becomes stable. Take for example the TWD frequency curve in Fig. 2(e). It starts out at the stability threshold r_{stab}^D—being for $k=\pi$ and small Re only very slightly above the Re$=0$ threshold r_{osc}— with a frequency at onset, ω_{stab}^D, which is slightly throughflow enhanced relative to the Re$=0$ counterpart ω_H (cf Fig. 1). Following the TWD solution branch ω drops continuously to the asymptotic value $\omega \simeq 1$ at large r far beyond the old SOC-TW transition at r^*. This asymptotic frequency is given by the phase velocity of the downstream propagating former SOC pattern. Similarly the other TWD bifurcation curves for M and $N-1$ join smoothly at large r with the branch that has evolved out of the former SOC solution. This ‘‘downstream propagating SOC’’ at large r resembles strongly the one that one observes in a pure fluid, $\psi=0$, with lateral through flow: The TWD Nusselt number approaches at large r the $\psi=0$ Nusselt number marked by the dotted line in Fig. 2(f).

2. TWU's at small Re

When switching on a (small) through flow the solution branch of left propagating waves that bifurcates out of the conductive state with negative frequency, $\omega=-\omega_H$, evolves into the TWU solution marked in the right column of Fig. 2 by lines with upwards pointing triangles. It starts out at the TWU stability threshold r_{stab}^U—being for $k=\pi$ and small Re only very slightly below the Re$=0$ threshold r_{osc}—with a frequency at onset, ω_{stab}^U, which is slightly larger than its Re$=0$ counterpart (c.f. Fig. 1). Proceeding in Fig. 2 from the TWU onset along the TWU solution branch it becomes stable at the saddle marked by $U2$ in Fig. 2(e) and located at $r_{S2}^U \simeq 1.2$. It remains stable until the saddle $U3$ located at $r_{S3}^U \simeq 1.27$. There, the stable TWU solution connects with an unstable solution that has evolved out of the former upper unstable SOC branch with larger Nusselt number. This saddle connection evolves with increasing through flow out of the $\omega=0$ merging at Re$=0$ of the left propagating TW with the SOC at r^*. To summarize: for small Re the *stable* TWU connects at $U3$ with the *unstable* former SOC branch at $r<r^*$. On the other hand, the *stable* TWD solution that evolves out of the right propagating TW connects smoothly to the *stable* former SOC solution at $r>r^*$.

With increasing Re the saddles $U3$ and $U2$ collide, and one is left then with a solution branch of unstable TWU's having the saddle $U1$ only. This saddle $U1$ located in the right column of Fig. 2 at $r_{S1}^U \simeq 1.08$ originates from the former SOC saddle at $r_S^{SOC} \simeq 1.078$ in the left-hand column of Fig. 2. Hence its location is not much influenced by the through flow of Fig. 2.

The TWU frequency increases monotonically when following the TWU solution branch from onset at r_{stab}^U to its large-r asymptote. The asymptotic TWU frequency of this unstable, small-amplitude traveling wave is slightly below the asymptotic frequency of the stable, large-amplitude TWD at large r far beyond the old TW-SOC transition.

The Nusselt number differences between TW's, TWU's, and TWD's [Fig. 2(c) and Fig. 2(f)] are small. In accordance to the model of Hollinger *et al.* [54] larger oscillation frequencies of TWD's are associated with smaller convective amplitudes and therefore with smaller Nusselt numbers compared to those of TWU's. Comparing the mixing parameter M [Figs. 2(a) and 2(d)] one observes for TWU's a strong increase in M near r_{S3}^U.

3. Hysteresis by changing r and Re

In the presence of through flow there arise different combinations of existence ranges of TW's. There is an r range where only TWU's are stable, $r_{S2}^U \leqslant r < r_S^D$, and an r range where only TWD's are stable, $r_{S3}^U \leqslant r$. For $\psi=-0.25$ and Re$=0.075$ the range $[r_{S2}^U, r_{S3}^U]$ of existence of stable TWU's is separated from the range of existence of stable TWD's, $r > r_S^D$. In between there arises a small r regime where neither TWD nor TWU states are stable.

For Re$=0$ only a hysteresis between the basic state and convective states exists for $r_S^{TW} < r < r_{osc}$ if one increases or decreases the Rayleigh number. In the presence of through flow there exists an additional hysteresis of TW convection for a combined change of r and Re. For Re$=0.075$ one has $r_{S3}^U < r_S^D$ for $\psi=-0.25$; in between this interval neither TWD's nor TWU's are stable. Consider as a start the stable TWU at $r \simeq 1.25$, Re$=0.025$. If one now first reduces r to $r \simeq 1.20$ and then increases the Reynolds number to Re $=0.075$ one still observes a stable TWU. On the other hand, if one first increases the Reynolds number to Re$=0.075$ one causes a transition TWU→TWD. This TWD state then becomes unstable when reducing the Rayleigh number to $r \simeq 1.20$. In this case only the basic state is established.

4. Dependence on ψ and Re

In Figs. 3 and 4 oscillation frequency ω, mixing parameter M, and Nusselt number $N-1$ are shown as functions of r for increasing through flow rates (Re$=0$, 0.05, 0.1, 0.25) and three different Soret coupling strengths ($\psi=-0.01$, -0.1, -0.25).

With increasing through flow the frequency of TWD's increases. In addition the convective amplitude and the Nusselt number decreases whereas the Rayleigh number of the TWD saddle, r_S^D, increases. The TWD bifurcation behavior described in Sec. IV C 1 for $\psi=-0.25$, Re$=0.025$ remains

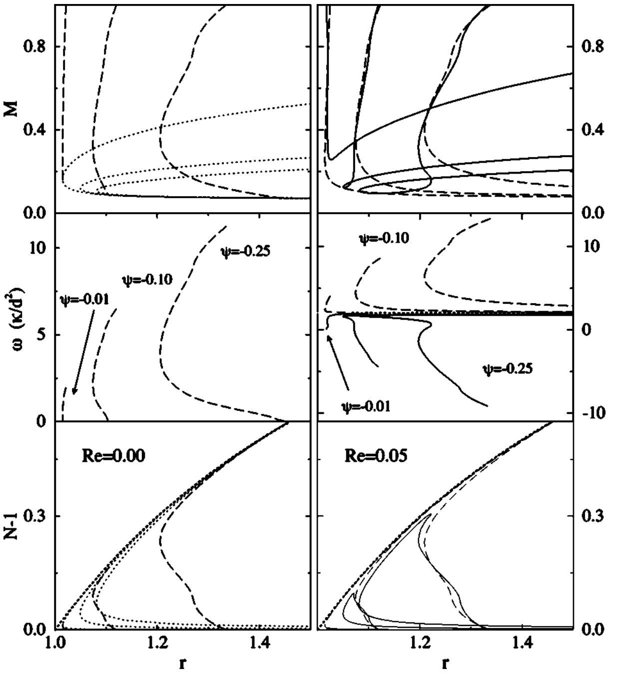

FIG. 3. Influence of lateral through flow on bifurcation properties of roll convection for different Soret coupling strengths ψ as indicated. Shown are, from top to bottom, mixing number M, frequency ω, and Nusselt number $N-1$ versus reduced Rayleigh number r at $\mathrm{Re}=0$ (left column) and at $\mathrm{Re}=0.05$ (right column). Right propagating TW's at $\mathrm{Re}=0$ and TWD's at $\mathrm{Re}=0.05$: dashed lines. TWU's at $\mathrm{Re}=0.05$: full lines. SOC at $\mathrm{Re}=0$: thin, dotted lines. Nusselt numbers in pure fluids ($\psi=0$): thick, dotted lines. The stability of the solutions can be inferred from Fig. 2 using the fact that it changes at the saddles. Parameters are $L=0.01$, $\sigma=10$, $k=\pi$.

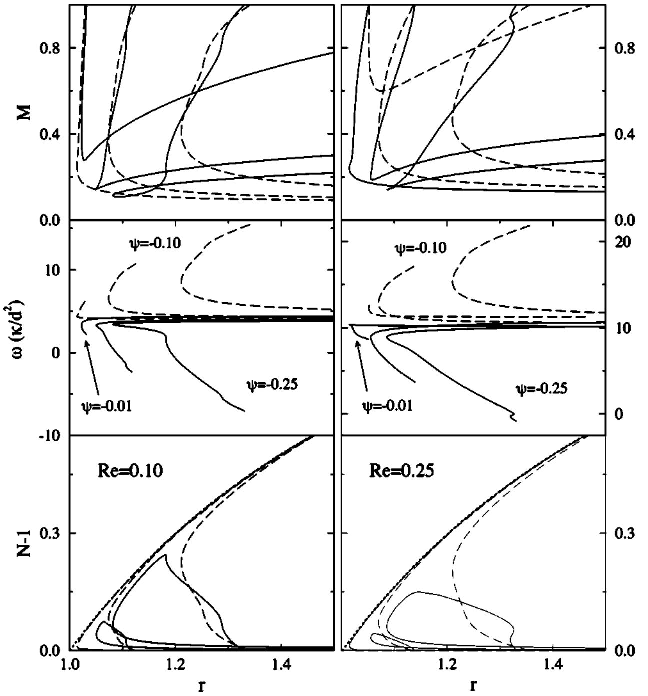

FIG. 4. Influence of lateral through flow on bifurcation properties of roll convection for different Soret coupling strengths ψ as indicated. Shown are, from top to bottom, mixing number M, frequency ω, and Nusselt number $N-1$ versus reduced Rayleigh number r at $\mathrm{Re}=0.1$ (left column) and at $\mathrm{Re}=0.25$ (right column). TWD's: dashed lines; TWU's: full lines; Nusselt numbers in pure fluids ($\psi=0$): thick, dotted lines. The stability of the solutions can be inferred from Fig. 2 using the fact that it changes at the saddles. Parameters are $L=0.01$, $\sigma=10$, $k=\pi$.

qualitatively unchanged at other Soret coupling ψ or other through flow rates. This is most easily seen from the fact that the bifurcation topology of the dashed TWD curves in Figs. 3 and 4 is the same as that of the respective TWD solutions (lines with downwards pointing triangles) in the right column of Fig. 2.

A growing through flow shifts the TWU saddle $U3$ towards smaller r, thus reducing the range of existence of stable TWU's further and further. For $\psi=-0.25$ and $\mathrm{Re}=0.01$ one still sees the $U3$ saddle at $r_{S3}^{U}<r_{c}^{U}$. In addition r_{S2}^{U} is shifted to smaller r-values with increasing through flow rates. At $\mathrm{Re}\simeq 0.08$ the saddles $U2$ and $U3$ merge and the range of existence of stable TWU's disappears for $\psi=-0.25$.

Consider now the separation ratio $\psi=-0.01$: At $\mathrm{Re}=0.1$ one has $r_{stab}^{D}<r_{stab}^{U}$ [see Fig. 1(a) for the critical thresholds]. Then, with increasing through flow rates both stability thresholds cross and finally one obtains $r_{stab}^{U}<r_{stab}^{D}$ at large Re. Between $\mathrm{Re}=0.10$ and $\mathrm{Re}=0.25$ (Fig. 4) the former TWU branch, connecting r_{stab}^{U} with r_{stab}^{S}, transforms into a TWD branch indicated by a change in the linestyle in the figures. For $\mathrm{Re}=0.25$ the unstable TWD branch (dashed line in Fig. 4) starting from the onset $r_{stab}^{D}\simeq 1.05$ folds back to the basic state at $r_{stab}^{S}\simeq 1.47$. At $\mathrm{Re}=0.5$ the linear thresholds r_{stab}^{D} and r_{stab}^{S} have already disappeared [see also Fig. 1(a)]. The whole TWD branch vanishes, and one only observes TWU solutions starting from r_{stab}^{U}, which are now again stable for Rayleigh numbers above the unique saddle r_{S}^{U}.

D. Wave number dependence

So far we have investigated in this Sec. IV patterns with wave number $k=\pi$. However, in experiments using narrow convection channels with large aspect ratios, $\Gamma \gg 1$, different convective patterns of spatially uniform amplitude with different wavelengths are possible. We therefore elucidate here the wave number dependence of the order parameters too and discuss our main results for such patterns of spatially uniform amplitude.

1. Absence of through flow

In Fig. 5 the bifurcation branches of the Nusselt numbers of TW and stable SOC states are plotted for $\mathrm{Re}=0$ and equidistantly spaced k. These curves were determined with our many-mode Galerkin scheme described in Sec. II D. The bifurcation surface of $N-1$ over the $r-k$ plane branches out of the latter at the marginal stability curve $r_{stab}^{TW}(k)$ (thick full line in Fig. 5) where $N-1\rightarrow 0$. This threshold for onset of convection increases whith increasing deviation of the wave number from k_{c}^{TW}. The thick dotted line connects the saddles $r_{S}^{TW}(k)$. They also move to larger r for larger and smaller wave numbers compared to a minimum value close to k_{c}^{TW}.

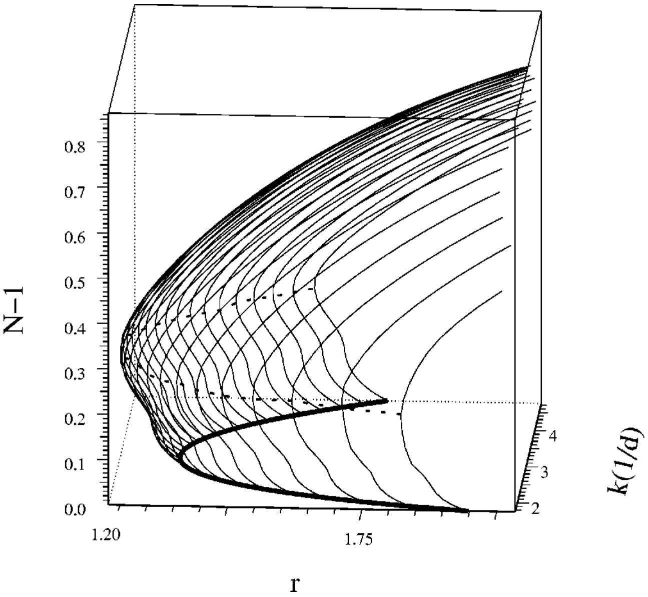

FIG. 5. Bifurcation surface of Nusselt number $N-1$ in the absence of through flow over the r-k plane. Thin lines show cuts at equidistantly spaced k values. Two symmetry degenerate left and right propagating TW solutions with wave number k branch out of the conductive state at the stability threshold $r_{stab}^{TW}(k)$ (thick full line) where $N \rightarrow 1$. The initially unstable TW's become stable at the saddle $r_S^{TW}(k)$ (thick dotted line). Parameters are $L=0.01$, $\sigma=10$, $\psi=-0.25$, Re=0.

All in all, the surface of the order parameter $N(r,k)-1$ in Fig. 5 resembles that of a nose.

To discuss the wave number dependence of the order parameters we present in Fig. 6 cuts through the surfaces of $N(r,k)$, $\omega(r,k)$, and $M(r,k)$ at constant r values. For orientation we show in Fig. 6(a) the marginal stability curve $r_{stab}^{TW}(k)$ (thick line) and the position of the saddle $r_S^{TW}(k)$ (dotted line) for zero through flow. The hysteresis range, $r_{stab}^{TW}(k)-r_S^{TW}(k)$, of TW's has a nearly k independent width and moves to higher r values when $|k-k_c^{TW}|$ increases.

In the hysteretical region, $r_S^{TW} \leqslant r < r_{stab}^{TW}$, the bifurcation branches taken at fixed r as functions of k are closed in itself. Stable and unstable branches are joined together at the saddle $r_S^{TW}(k)$ (dotted lines in Fig. 6) at a small and a large wave number. At these saddle connections one observes strong variations of all order parameters over the r-k plane.

Stable TW's are located in the bifurcation diagrams of Fig. 6(b) above, in Fig. 6(c) between, and in Fig. 6(d) below the dotted saddle lines. With increasing r the k range of stable TW solutions widens. *Unstable* TW's are located between the dotted saddle lines and the onset out of the basic state marked by $N-1=0$ in Fig. 6(b), $\omega = \pm \omega_{stab}^{TW}(k)$ (thick full lines) in Fig. 6(c), and $M=1$ in Fig. 6(d). For a fixed r above the minimum of $r_{stab}^{TW}(k)$, the unstable TW solution branches are connected to the basic state at the two k values where $r=r_{stab}^{TW}(k)$—see, e.g., the curves of $N-1$ versus k in Fig. 6(b). Increasing r beyond, say, $r=1.275$ the unstable branches start to buckle before they reach the basic state at $r=r_{stab}^{TW}(k)$ and then split apart.

The Nusselt number is a nearly symmetric function of $k-k_c^{TW}$. The onset frequency, $\omega_{stab}^{TW}(k)$ [upper thick line in Fig. 6(c)], of the right propagating TW increases monotonically with k showing normal dispersion. Also the frequency of the saddle TW at $r_S^{TW}(k)$ increases with k along the dotted saddle line in Fig. 6(c), however, with a smaller growth rate. Similarly, the mixing parameter M of the saddle TW decreases as a function of k along the dotted saddle line in Fig. 6(d). Due to convective mixing the frequency of stable TW's is much smaller than the critical frequency $\omega_{stab}^{TW}(k)$.

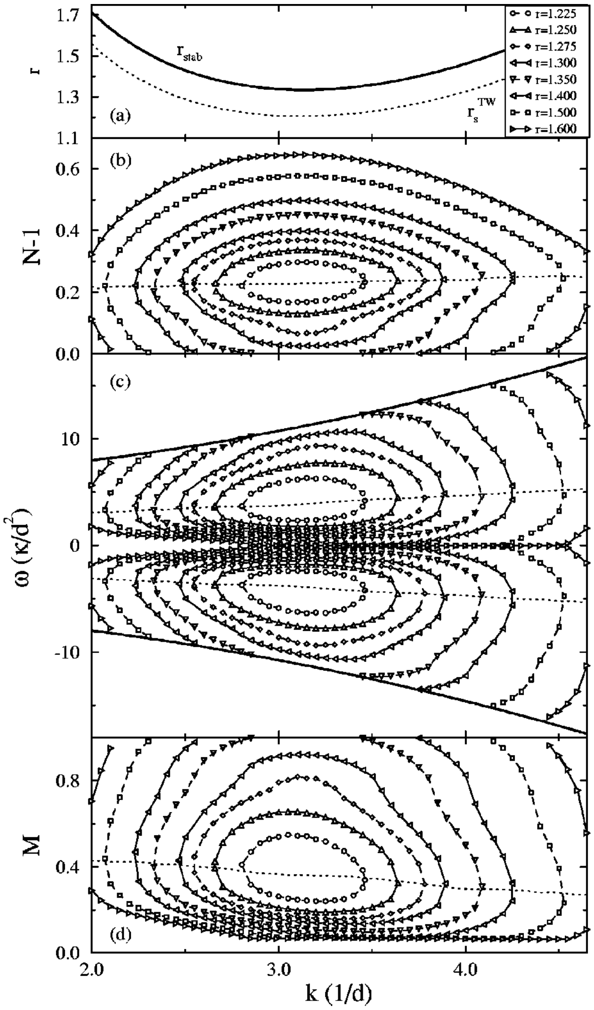

FIG. 6. Wave number dependence of order parameters $N-1$ (b), ω (c), and M (d) in the absence of through flow at different r values. For orientation we show in (a) the bifurcation threshold $r_{stab}^{TW}(k)$ (thick full line) and the saddle location $r_S^{TW}(k)$ (dotted line). Thick full curves in (c) denote frequencies, $\pm \omega_{stab}^{TW}(k)$, of right and left propagating TW's at onset, $r_{stab}^{TW}(k)$. Saddle values of the order parameters are marked in (b), (c), and (d) by dotted lines. TW solutions are unstable between onset and saddle. Stable TW's are located in (b) above, in (c) between, and in (d) below the dotted saddle lines. Parameters are $L=0.01$, $\sigma=10$, $\psi=-0.25$, Re=0.

At a fixed r the group velocity, $v_g=\partial_k \omega$, of stable (unstable) right propagating TW's is negative (positive) for small k, changes sign around $k \simeq k_c^{TW}$, and becomes positive (negative) for larger k. Furthermore, for a fixed r the group velocity of the two saddle TW's diverges at the two intersections of the frequency curves in Fig. 6(c) with the dotted saddle line. The phase velocity $v_p=\omega/k$ is always positive. At the SOC-TW transition, $r^*(k)$, the TW solution branches merge with zero frequency with the stable SOC branches of the different k's.

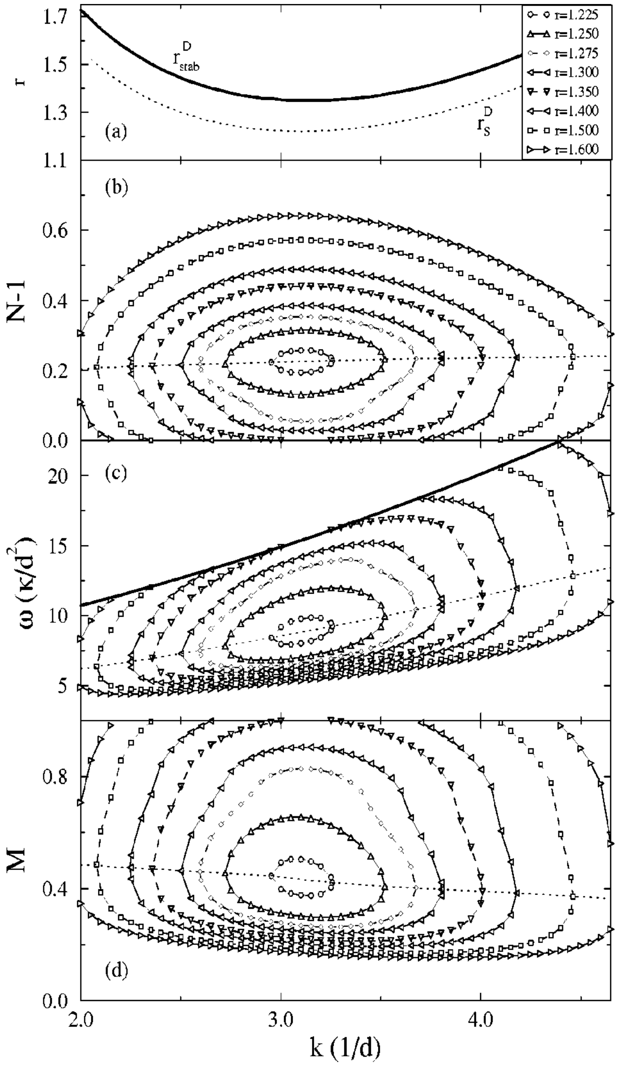

FIG. 7. Wave number dependence of TWD order parameters $N-1$ (b), ω (c), and M (d) in the presence of a small through flow at different r values. For orientation we show in (a) the bifurcation threshold $r^D_{stab}(k)$ (thick full line) and the saddle location $r^D_S(k)$ (dotted line). Thick full curve in (c) denotes the TWD frequency $\omega^D_{stab}(k)$ at onset $r^D_{stab}(k)$. Saddle values of the order parameters are marked in (b), (c), and (d) by dotted lines. TWD's are unstable between onset and saddle. Stable TWD's are located in (b) above and in (c) and (d) below the dotted saddle lines. Parameters are $L=0.01$, $\sigma=10$, $\psi=-0.25$, Re=0.1.

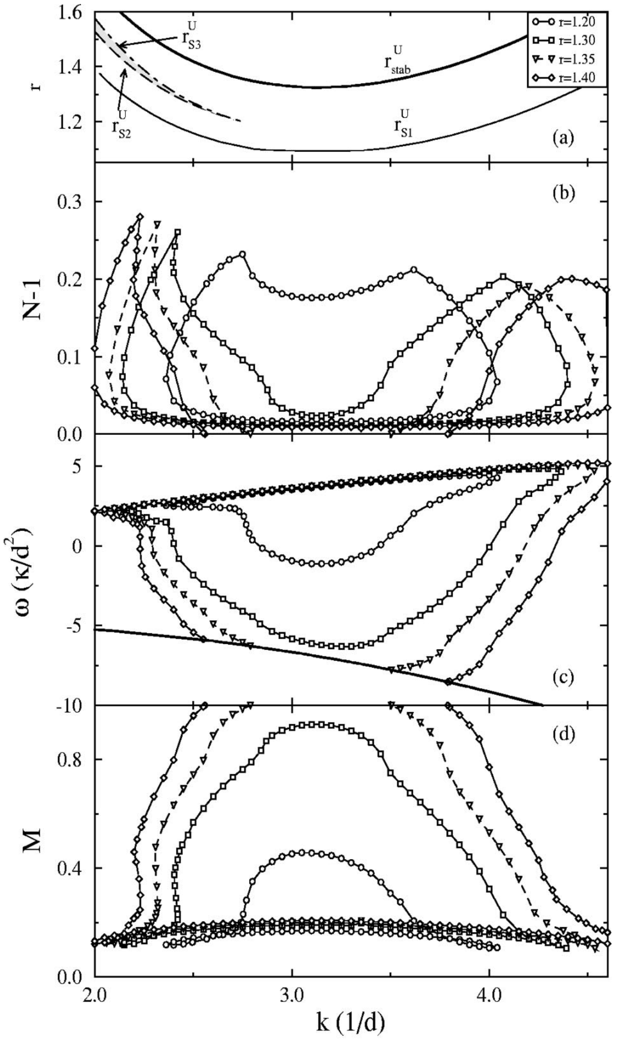

FIG. 8. Wave number dependence of TWU order parameters $N-1$ (b), ω (c), and M (d) in the presence of a small through flow at different r values. For orientation we show in (a) the bifurcation threshold $r^U_{stab}(k)$ (thick full line) and the saddle locations $r^U_{S1}(k)$, $r^U_{S2}(k)$, and $r^U_{S3}(k)$. The thick full curve in (c) denotes the TWU frequency $\omega^U_{stab}(k)$ at onset $r^U_{stab}(k)$. Stable TWU's occur only in the narrow shaded interval bounded by the saddle lines r^U_{S2} and r^U_{S3} shown in (a). Parameters are $L=0.01$, $\sigma=10$, $\psi=-0.25$, Re=0.1.

2. Finite through flow: TWD's

The wave number dependence of the TWD order parameters at several fixed r values is shown in Fig. 7 for a small through flow, Re$=0.1$. The presentation is the same as that of Fig. 6 for TW's at zero through flow except that in Fig. 7(c) only the positive frequency range of TWD's is shown. Also here the hysteresis range of TWD's between the marginal stability curve $r^D_{stab}(k)$ [thick full line in Fig. 7(a)] and the saddle $r^D_S(k)$ [dotted line in Fig. 7(a)] moves with nearly independent width to higher r values when $|k-k^D_c|$ increases. Similar to TW's at Re$=0$, the TWD bifurcation branches taken at fixed r as functions of k are closed in themselves in the hysteretical region, $r^D_S \leqslant r \leqslant r^D_{stab}$, and stable and unstable branches are connected at the saddle $r^D_S(k)$ (dotted lines in Fig. 7) at a small and a large wave number, respectively.

Stable TWD's are located in Fig. 7(b) above and in Figs. 7(c) and 7(d) below the dotted saddle line. Here also the k range of stable TWD's widens with increasing r. However, since for finite through flow the onset $r^D_{stab}(k)$ and the saddle $r^D_S(k)$ are shifted upwards towards higher Rayleigh numbers the stable k interval for TWD's at fixed r has shrunk relative to the Re$=0$ situation. This is clearly visible in Fig. 7 near the dotted saddle lines. For example, at $r=1.225$ the size of the stable TWD interval for Re$=0.1$ is less than half its size for Re$=0$. And for Re$=0.25$ the saddle position $r^D_S(k)$ lies already completely above $r=1.225$. *Unstable* TWD's are located between the saddle lines and the onset marked by $N=1$ in Fig. 7(b), $\omega=\omega^D_{stab}(k)$ (thick full line) in Fig. 7(c), and $M=1$ in Fig. 7(d).

The Nusselt number curves of TWD's in Fig. 7(b) are not much changed by the through flow. However, the TWD frequencies show relative to their Re$=0$ counterparts in Fig. 6(b) an additional linear increase with k that is proportional to Re. This increase reflects the TWD pattern advection by the lateral throughflow. For Re$=0.25$ the advective frequency enhancement of large-k patterns is already so strong that one finds for a fixed r saddle TWD's with $k>\pi$ that have frequencies larger than the onset frequency $\omega^{D}_{stab}(k<\pi)$ at $k<\pi$. Note that the TWD frequency branches in Fig. 7(c) never approach $\omega=0$ unlike their Re$=0$ counterparts in Fig. 6(c): the through flow destroys the TW-SOC transition and the TWD patterns move at large r with an asymptotic finite frequency that roughly increases linearly with k.

The through flow increases the mixing parameters M of stable TWD's by a k independent amount, say, from $M\simeq 0.1$ at Re$=0$ to $M\simeq 0.2$ at Re$=0.25$.

3. Finite through flow: TWU's

The through flow has considerably more influence on left propagating TW's than on right propagating TW's. There may appear up to three saddles on the TWU solution branches that are identified for $k=\pi$ in Fig. 2 with increasing r by $U1$, $U2$, and $U3$. They make the wave number dependence of the bifurcation branches rather complicated.

In Fig. 8(a) we show the saddles $r^{U}_{S1}(k)$, $r^{U}_{S2}(k)$, and $r^{U}_{S3}(k)$ together with the marginal stability threshold $r^{U}_{stab}(k)$ as functions of k for Re$=0.1$. Stable TWU's exist for Re >0 only in the range $r^{U}_{S2}(k)\leqslant r\leqslant r^{U}_{S3}(k)$ that is finite only at small wave numbers and sufficiently small Re [cf. shaded area between the two saddle lines in Fig. 8(a)]. At higher through flows $r^{U}_{S2}(k)$ and $r^{U}_{S3}(k)$ merge, the stable TWU range is pinched off, and only unstable TWU's are left.

To understand the topology of the TWU solution branches at fixed r in Fig. 8 consider as an example the case $r=1.35$ lying slightly above r^{U}_{c} that is marked by downwards pointing triangles. The initially unstable TWU solution branches start for this particular r at onset with wave number $k\simeq 2.78$ with $N-1=0$ [Fig. 8(b)], $\omega=\omega^{U}_{stab}$ [at the full thick line in Fig. 8(c)], and $M=1$ [Fig. 8(d)]. Following the solution branches in Figs. 8(b)–8(d) with decreasing k the Nusselt number and the frequency grow while M decreases. Then, at the saddle $U2$ at $k\simeq 2.30$ the TWU solution branches are folded back to increasing wave numbers and the TWU's become stable. After passing the saddle $U3$ at $k\simeq 2.31$ where N is maximal the TWU's lose stability. Then one wanders with decreasing k and N along the former upper unstable SOC branch of $N-1$ down to the saddle $U1$ at $k\simeq 2.05$. After that the wave number increases while N continues to decrease to its minimum before it increases again on the way to the $U1$ saddle at large $k\simeq 4.53$. At the second maximum of $N-1$ at $k\simeq 4.22$ the former unstable lower SOC branch of the Nusselt number is again connected with the unstable TW branch, and one finally reaches the basic state again, now, however, with $k\simeq 3.50$.

In the absence of through flow the onset frequency of left propagating TW's, $-\omega^{TW}_{stab}(k)$ [lower thick full curve in Fig. 6(c)], is monotonically decreasing with k. Due to the through flow induced frequency enhancement—that increases almost linearly with k and Re—the group velocity of TWU's at onset, $\partial_k\omega^{U}_{stab}(k)$, is much smaller in Fig. 8(b) than in Fig. 6(b). Already for Re$=0.25$ the function $\omega^{U}_{stab}(k)$ is symmetric in $k-k^{U}_{c}$. But for such large through flow rates there exist only unstable TWU's.

V. TRANSIENTS

In this section we investigate (i) the growth dynamics out of infinitesimal perturbations of the conductive state into stable, strongly nonlinear TW's, (ii) the transition between a TWU and a TWD after changing the Rayleigh number, and (iii) the decay of TW's into the basic state. To analyze the transient dynamics we used among others lateral Fourier decompositions of the numerically obtained fields. In particular we consider the fields at midheight, $z=0$, of the layer

$$f(x,z=0;t)=\sum_{n=-\infty}^{\infty} f_n(t)e^{inkx}. \tag{5.1}$$

Here $f_{-n}=f^{*}_{n}$ since all fields f are real.

A. Growth dynamics

The initial growth dynamics out of the conductive state is dominated by the $n=1$ mode in Eq. (5.1). As long as deviations from the conductive state are still small enough they can be described by the linear equations (3.1). Then $f_1(t)$ takes according to Eqs. (3.2), (3.3) the form

$$f_1(t)=A_D e^{-i\omega_D t}e^{\gamma_D t}+A_U e^{-i\omega_U t}e^{\gamma_U t}. \tag{5.2}$$

Here $\omega_{D,U}$ are frequencies, $\gamma_{D,U}$ growth rates, and $A_{D,U}$ complex amplitudes of the TWD and TWU, respectively. We consider here a situation where r is larger than the bifurcation threshold of TWU as well as of TWD perturbations so that $\gamma_{D,U}>0$. Then both waves grow. However, their initial amplitudes A_D ,A_U as well as their growth rates γ_D , γ_U and their frequencies ω_D , ω_U will in general be different. Consequently the contribution of the $n=1$ mode (5.2) to the fields (5.1) yields with $\omega_D>0$ and $\omega_U<0$ a rather complicated superposition of downstream (right) and of upstream (left) traveling waves. For convenience we use the indices D and U also in the case of zero through flow to identify right and left traveling waves, respectively.

1. Absence of through flow

For a detailed discussion of the growth dynamics for Re $=0$ we refer to [10,56,57]. Here we review only the most important results to understand on this basis the effect of through flow. We should also like to mention that in experiments using large convection cells amplitude profiles and phases of perturbations are inhomogenous, and one observes complicated spatiotemporal dynamics [58–60,26,17]. Here we consider a setup with a separation ratio $\psi=-0.25$ and a lateral periodicity length of $\Gamma=\lambda=2$ with periodic boundary conditions thus enforcing a spatially uniform amplitude profile.

For Re$=0$ the eigenvalue problem for linear TW perturbations of the conductive state is symmetry degenerate with $\omega^{0}_{U}=-\omega^{0}_{D}$ such that right and left propagating perturbations of the basic state have the same growth rate, $\gamma^{0}_{D}=\gamma^{0}_{U}$. However, depending on initial conditions, the amplitudes A^{0}_{D} and A^{0}_{U} of the two counterpropagating waves will in general be

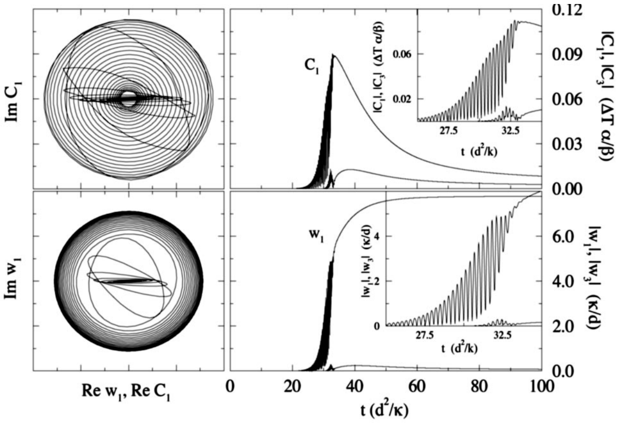

FIG. 9. Growth dynamics of lateral Fourier modes at midheight of the fluid layer for Re $=0$. Initial condition is the basic state with small noise of $O(10^{-4})$ superimposed onto the conductive temperature field. Left column shows in a pointer diagram the complex amplitudes C_1 and w_1 in the complex amplitude plane. Right column shows time dependence of the moduli of the Fourier modes. Parameters are $L=0.01$, $\sigma=10$, $\psi=-0.25$, r$=1.418$, $k=\pi$.

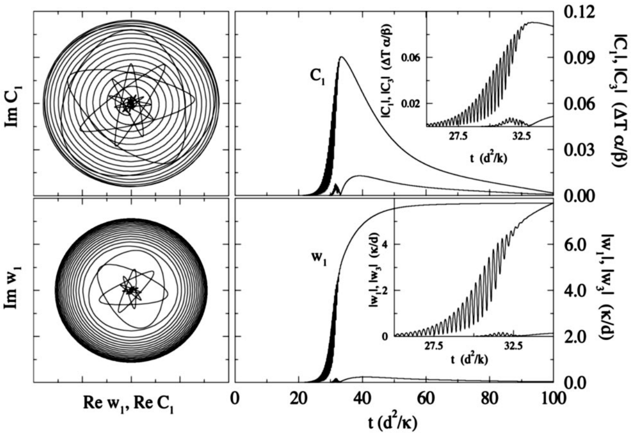

FIG. 10. Growth dynamics of lateral Fourier modes at midheight of the fluid layer for Re $=0.025$. Otherwise the conditions and quantities are the same as in Fig. 9.

different. For $A_U^0=0$ or $A_D^0=0$ one would have a pure TW and for $|A_D^0|\simeq|A_U^0|$ one would have a standing wave (SW) with amplitudes that are growing exponentially.

In Fig. 9 we show the dynamics of the lateral Fourier harmonics w_1, w_3 of the velocity field and C_1, C_3 of the concentration field at midheight of the cell. The initial state consists of the basic state, with random perturbations of the temperature field of $O(10^{-4})$ added to it. The Rayleigh number $r=1.418$ is slightly above the oscillatory threshold $r_{osc}=1.3348$. In the linear growth regime up to about $t=30$ one observes the growth dynamics of an almost ideal SW since the random noise provides amplitudes, A_D^0 and A_U^0, for right and left traveling waves, that are roughly of the same magnitude.

In the pointer diagrams (left columns of Fig. 9) we show the dynamics of the complex modes C_1 and w_1 in the complex plane. In this plot the initial SW shows up as an oscillation along a straight line through the origin. Nonlinear interaction between the two counterpropagating waves that combine to the SW causes faster growth of the one with the larger initial amplitude—in the case of Fig. 9 the left propagating TW. This causes a transition from SW to pure TW. It manifests itself in the pointer diagram of w_1 as a transition from a straight line via a spiral with counterclockwise motion in outwards direction as long as $|w_1|$ increases to a final circular motion for the relaxed left propagating TW. The initial contribution of the right traveling wave gets totally depressed by the nonlinear interaction with the predominating left traveling wave.

The amplitude of C_1 strongly overshoots for reasons related to the breaking of the large-amplitude standing concentration wave [10,57]. It reaches its maximal value at $t\simeq 33$ and afterwards decreases very slowly to its final value. The latter behavior is caused by convective mixing combined with diffusive homogenization to spatially constant plateau values in regions of closed streamlines in the comoving frame of reference of the TW, when the convection amplitude has become sufficiently large. This concentration redistribution causes the decrease of the oscillation frequency [10,57].

2. Presence of through flow: Competition between TWD and TWU

A small through flow breaks the symmetry degeneracy of the Hopf bifurcation. Bifurcation thresholds, frequencies, and growth rates of TWD's and TWU's are different. For the parameters considered here we have $|\omega_D|>|\omega_U|$, and $\gamma_D<\gamma_U$ in the growth regime.

If one considers an initial situation with $|A_D|\simeq|A_U|$ then a TWU will grow predominantly due to its larger growth rate. One should therefore observe a phase propagation in opposite direction to the through flow. But since $|\omega_D|>|\omega_U|$ there is for small amplitudes an additional downstream phase propagation in through flow direction. However, this TWD contribution weakens further and further during the nonlinear interaction regime until the TWD is totally depressed by the predominantly growing TWU.

Such a scenario occurs in Fig. 10. Here, for Re $=0.025$, $r=1.418$, the temporal growth rates $\gamma_U\simeq 0.39$ and $\gamma_D\simeq 0.37$ are slightly different, and $\omega_U\simeq-10.42$ while $\omega_D\simeq 12.51$. These growth rates and frequencies of TWU's and TWD's were obtained from a linear analysis. In the pointer diagram of w_1 the initial SW motion along a straight line that occured in Fig. 9 for Re $=0$ with equal growth rates and frequencies is here, in Fig. 10, replaced by the predominant evolution of the TWU that is perturbed by modulations from the TWD contribution with larger frequency. The latter die out soon and then an evolution towards a pure TWU takes place. However, for the parameters (Re $=0.025$, $r=1.418$, $\psi=-0.25$) of Fig. 10 the through flow does not admit a final, stable TWU state (cf Fig. 2)—the nonlinear TWU shown in Fig. 10 up to $t=100$ is only transient. It transforms after another 200–300 vertical thermal diffusion times into a stable TWD.

For a ten times larger through flow, Re $=0.25$, one has $\gamma_U\simeq 0.43$, $\gamma_D\simeq 0.22$, $\omega_U\simeq-1.08$, $\omega_D\simeq 22.03$. Then a TWD contribution to the intial linear growth dynamics is no longer visible in Fig. 11. So initially there is only the TWU growing. But for this large through flow the phase propagation reversal into a TWD occurs already at $t\simeq 35$ (cf. the pointer

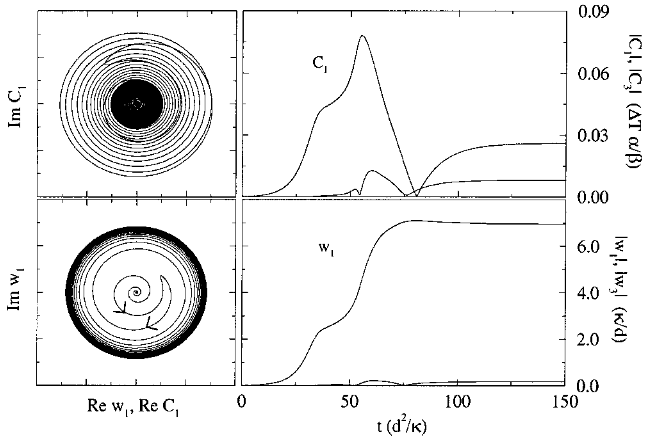

FIG. 11. Growth dynamics of lateral Fourier modes at midheight of the fluid layer for Re = 0.25. Otherwise the conditions and quantities are the same as in Fig. 9.

diagram of w_1 in Fig. 11). Thereafter the system relaxes into the stable nonlinear TWD state. Thus, initially TWU's win the growth competition but finally only TWD's will survive.

B. Dynamics at the transition TWU→TWD

Here we investigate the TWU→TWD transition with a reversal of the phase propagation. The problem of realizing a TWD→TWU transition is discussed in Sec. V C. The transition from a stable TWU that exists in the interval $r \in [r_{S2}^U, r_{S3}^U]$ to a stable TWD can be enforced by increasing the Rayleigh number to $r > r_{S3}^U$ beyond the $U3$ saddle. The dynamics of this transition is shown in Figs. 12 and 13.

In Fig. 12 we show the reaction of the order parameters N, ω, and M as a function of time during the transition TWU→TWD for the small through flow Re = 0.025. The transition was initiated at $t = 0$ by instantaneously increasing the Rayleigh number from $r \simeq 1.25$ to $r \simeq 1.27$ shortly beyond the $U3$ saddle. Then, with a fast initial transient on the time scale of a few thermal diffusion times, the convective flow adopts to the larger thermal driving which leads to an increase of the Nusselt number and of the convective flow intensity. The associated increase of the advective redistribution and mixing of the concentration field causes M and $|\omega_U|$ to decrease.

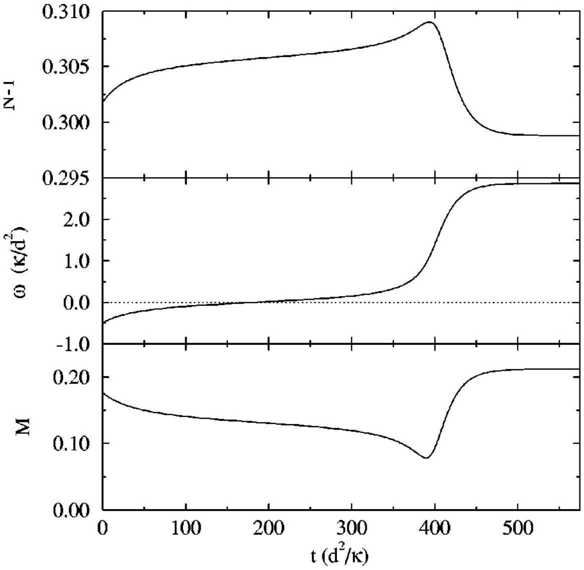

FIG. 12. Time evolution of order parameters $N-1$, ω , and M at transition TWU → TWD initiated at $t = 0$ by an instanteneous step $r \simeq 1.25 \rightarrow 1.27$ beyond the $U3$ saddle. Parameters are $L = 0.01$, $\sigma = 10$, $\psi = -0.25$, $k = \pi$, Re=0.025.

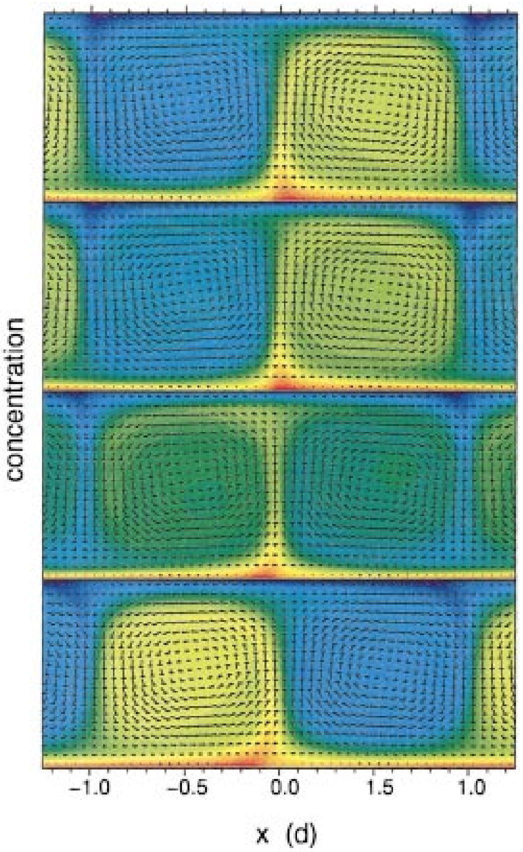

FIG. 13. (Color) Time evolution of concentration and velocity fields shown in color coded and vector field plots, respectively, during the transition TWU → TWD described in Fig. 12. Snapshots were taken every 200 vertical thermal diffusion times from top to bottom. Top plot is the TWU at $t = 0$, bottom plot the final TWD at 500 vertical thermal diffusion times. Red (blue) color implies low (high) concentration.

As was pointed out in the last section the oscillation frequency is coupled to finite phase shifts of mode amplitudes. A reversal of the phase propagation direction causes a change of sign of the phase differences between the mode amplitudes. At the transition TWU→TWD (i) phase shifts pass through zero in order to reverse the phase propagation direction or (ii) mode amplitudes vanish to allow for phase jumps. Here the phase φ_{T_1} of T_1 approaches nearly linearly the phase φ_{w_1} of w_1. Crossing the zero line of $\varphi_{T_1} - \varphi_{w_1}$ at $t \simeq 400$ in Fig. 12 happens at the same time when a phase jump of $\varphi_{C_1} - \varphi_{w_1}$ occurs which indicates that C_1 vanishes. After that the system relaxes into the stable final TWD state at about 500 vertical thermal diffusion times.

A more detailed visualization of the transition TWU→TWD is shown in Fig. 13. There we show successive snapshots of the concentration field and of the velocity field taken every 200 vertical thermal diffusion times. At $t = 0$

(top of Fig. 13) the stable TWU is shown before we have increased the Rayleigh number. There the left, counterclockwise circulating roll has a higher concentration level than the right, clockwise circulating roll. Due to the phase difference between velocity and concentration field the concentration plateaus are asymmetrically fed by the boundary layers at the plates [31,9,10]. At $t \simeq 200$ (second picture of Fig. 13) the oscillation frequency determined via the temporal derivative of φ_{T_1} vanishes. In contrast to that the phase difference $\varphi_{C_1} - \varphi_{w_1}$ has changed only slightly and reaches π only around $t \simeq 400$ (third picture of Fig. 13). At this particular time the boundary layers between the rolls are located right at the positions of maximal up- and downflow so that the concentration plateaus are fed symmetrically by the boundary layers at the plates. The concentration equilibrates due to the strong convective mixing before the phase difference $\varphi_{C_1} - \varphi_{w_1}$ changes sign. Thereafter the left, counter clockwise circulating roll is fed predominantely from the bottom plate with low concentration values whereas the right, clockwise circulating roll is fed from the top plate, and a large concentration contrast between adjacent rolls is reestablished when the system finally relaxes to the TWD state (last picture of Fig. 13).

C. Decay dynamics of TW's

Here we briefly discuss the transition from propagating convective roll patterns into the basic state when decreasing the Rayleigh number below the saddles that delimit the range of existence towards small r values.

In the absence of through flow such a situation occurs when decreasing r below r_S^{TW}. In our MAC simulation for $\psi = -0.25$, $L = 0.01$, $\sigma = 10$, $k = \pi$ we have instantaneously changed the Rayleigh number from $r = 1.25$ to $r = 1.20 < r_S^{TW}$. After reducing the thermal driving the convection amplitude and the Nusselt number decrease during a fast transient. Caused by the reduced convection amplitude the mixing of the concentration field weakens and the mixing parameter M and the oscillation frequency increases. After this fast transient N decreases slowly over a period of 100 vertical diffusion times whereas M increases further. At this time the mixing parameter reaches its maximum value at a frequency of $\omega \simeq 7$. This slow process is followed by a fast decay of all field amplitudes when the system relaxes into the basic state. During the whole transient of decay the TW with the opposite phase propagation direction, which is linearly damped for $r < r_{osc}$, is not excited, so we have a pure TW decay into the basic state.

We also investigated the decay dynamics of TWD's as well as of TWU's for finite through flow rates. They both show similar behavior compared to the dynamics in the absence of through flow described above. In the presence of through flow there can exist a situation where $r_{S2}^U < r < r_S^D$. Here, a transition TWD→TWU seems possible, at least in principle, when the Rayleigh number remains above the $U2$ saddle at r_{S2}^U. But such a transition from a TWD to a TWU has never occurred in the numerical MAC simulations. Due to their higher frequencies TWD's have smaller convection amplitudes compared to TWU's. A decrease into the Rayleigh number band (r_{S2}^U, r_S^D) further decreases the convection amplitude and in addition increases the frequency. Both processes drive the TWD further away from the stable TWU and cause instead a decay into the stable basic state rather than a transition to the stable TWU.

VI. CONCLUSION

The effect of a horizontal through flow with small Reynolds number on stationary and traveling wave convective patterns of rolls oriented perpendicular to the through flow has been investigated numerically with a Galerkin expansion and a finite-difference method. We first have reviewed linear bifurcation properties and in particular the through flow-induced symmetry breaking of the oscillatory instability. Then the influence of a through flow on nonlinear bifurcation properties is elucidated as a function of Re for several negative Soret coupling strengths ψ. Also the wave number dependence of the bifurcation properties of the order parameters mixing number M, Nusselt number N, and oscillation frequency ω has been determined.

The through flow causes stationary patterns to propagate and furthermore lifts the symmetry degeneracy between left and right propagating TW's at $\mathrm{Re}=0$. The right (left) propagating wave with positive (negative) frequency at $\mathrm{Re}=0$ becomes a downstream (upstream) propagating TWD (TWU) in the presence of a small through flow. Not only the onset Rayleigh number and initial frequency of TWD and TWU differ but more importantly the symmetry degenerate zero-frequency merging of the two TW's with the SOC occurring for $\mathrm{Re}=0$ at r^* is dramatically changed by the through flow. In the absence of through flow the transition from the two stable symmetry degenerate TW states at $r < r^*$ to a stable SOC at $r \geqslant r^*$ marks a drift instability of the latter towards the former. The pitchfork topology of the associated bifurcation diagram of ω versus r close to r^* is changed to a shifted, imperfect bifurcation by the through flow: It breaks the left-right symmetry leading to a breakup and reconnection of the TW-SOC connections at r^*. In addition the phase velocities, i.e., the frequencies of the two TW's are shifted upwards. For small Re the TWU solution branch gets connected with the *unstable* former SOC branch at $r < r^*$. On the other hand, the *stable* TWD solution that evolves with increasing through flow out of the right propagating TW connects smoothly to the *stable* former SOC solution at $r > r^*$.

In the last section we have investigated the growth dynamics from infinitesimal perturbations of the conductive state into stable, strongly nonlinear TW's, the transition between a TWU and a TWD after changing the Rayleigh number, and the decay of TW's into the basic state. For $\mathrm{Re}=0$ right and left propagating perturbations of the basic state have the same growth rate. So for ''generic'' initial perturbations for which the amplitudes of the two counterpropagating waves are small and *roughly* the same one observes initially an exponentially growing standing wave. The nonlinear interaction between the two counterpropagating waves that combine to the SW causes faster growth of the one with the larger initial amplitude and finally a pure right or left propagating TW occurs. In the presence of a small through flow, bifurcation thresholds, frequencies, and growth rates of TWD's and TWU's are different. For ''generic'' initial perturbations a TWU will grow due to its larger growth rate thereby suppressing any TWD admixture. However, the stability range of final-state nonlinear TWD's is typically much larger than the one of TWU's. So for many parameters the system cannot run into a stable TWU. In such a situation one observes finally a tranformation of the transient TWU to a TWD.

The TWU→TWD transition with a reversal of the phase propagation being an interesting and experimentally realizable phenomen was investigated in more detail: In a TWU (TWD) the counterclockwise circulating roll has a higher (lower) concentration level than the clockwise circulating roll—due to the respective phase differences between *C* and *w* concentration is fed asymmetrically by the boundary layers at the plates into the two rolls. When the phase velocity reverses during the transition the vertical boundary layers between the rolls are located right at the positions of maximal up- and downflow so that the concentration is fed symmetrically into the rolls. The concentration equilibrates due to the strong convective mixing before the phase difference between *C* and *w* changes sign. Thereafter the system relaxes into the TWD state with a reverted concentration contrast between the rolls. Velocity and temperature fields do not change much during this transition.

ACKNOWLEDGMENTS

This work was supported by the Deutsche Forschungsgemeinschaft. The John von Neumann-Institut für Computing in Jülich provided computer time.

---

[1] M. C. Cross and P. C. Hohenberg, Rev. Mod. Phys. **65**, 851 (1993).

[2] Recent experimental results are presented, e.g., by A. Tsameret and V. Steinberg, Phys. Rev. E **49**, 1291 (1994); **49**, 4077 (1994); and by K. L. Babcock, G. Ahlers, and D. S. Cannell, *ibid.* **50**, 3670 (1994). A theoretical and numerical analysis can be found in P. Büchel, M. Lücke, D. Roth, and R. Schmitz, *ibid.* **53**, 4764 (1996).

[3] J. M. Luijkx, J. K. Platten, and J. C. Legros, Int. J. Heat Mass Transf. **24**, 1287 (1980).

[4] J. K. Platten and J. C. Legros, *Convection in Liquids* (Springer-Verlag, Berlin, 1984).

[5] H. W. Müller, M. Lücke, and M. Kamps, Europhys. Lett. **10**, 451 (1989).

[6] R. E. Kelly, Adv. Appl. Mech. **31**, 35 (1994).

[7] The few early works are reviewed in Ref. [4]. Reference [27] presents a comprehensive, numerically exact stability analysis of the basic nonconvecting state consisting of lateral Poiseuille flow with horizontal stratification of temperature and concentration.

[8] For a review see Refs. [4,1]. Further references may be found, e.g., in Refs. [9,10]. See also the more recent publications [11–17] of some of the many groups that have investigated convection in binary mixtures.

[9] W. Barten, M. Lücke, M. Kamps, and R. Schmitz, Phys. Rev. E **51**, 5636 (1995); **51**, 5662 (1995).

[10] M. Lücke, W. Barten, P. Büchel, C. Fütterer, S. Hollinger, and Ch. Jung, in *Evolution of Structures in Dissipative Continuous Systems*, edited by F. H. Busse and S. C. Müller, Lecture Notes in Physics, Vol. m55 (Springer, Berlin, 1998), p. 127.

[11] E. Kaplan, E. Kuznetsov, and V. Steinberg, Phys. Rev. E **50**, 3712 (1994).

[12] P. Kolodner, Phys. Rev. E **50**, 2731 (1994).

[13] H. Touiri J. K. Platten, and G. Chavepeyer, Eur. J. Mech. B/Fluids **15**, 241 (1996).

[14] L. Ning, Y. Harada, and H. Yahata, Prog. Theor. Phys. **97**, 831 (1997).

[15] A. Spina, J. Toomre, and E. Knobloch, Phys. Rev. E **57**, 524 (1998).

[16] A. La Porta and C. M. Surko, Physica D **23**, 21 (1998).

[17] K. Lerman, D. S. Cannell, and G. Ahlers, Phys. Rev. E **59**, 2975 (1999).

[18] P. Büchel, Ph.D. thesis, Universität des Saarlandes, Saarbrücken, 1999.

[19] L. D. Landau and E. M. Lifshitz, *Fluid Mechanics* (Pergamon Press, Oxford, 1959).

[20] P. Kolodner, H. L. Williams, and C. Moe, J. Chem. Phys. **88**, 6512 (1988).

[21] W. Hort, S. J. Linz, and M. Lücke, Phys. Rev. A **45**, 3737 (1992).

[22] J. Liu and G. Ahlers, Phys. Rev. E **55**, 6950 (1997).

[23] G. W. Baxter, K. D. Eaton, and C. M. Surko, Phys. Rev. A **46**, R1735 (1992); P. Kolodner, *ibid.* **46**, R1739 (1992); **46**, 6431 (1992).

[24] P. Kolodner, Phys. Rev. A **46**, 6452 (1992).

[25] E. Kaplan and V. Steinberg, Phys. Rev. Lett. **71**, 3291 (1993).

[26] A. La Porta and C. M. Surko, Phys. Rev. E **56**, 5351 (1997).

[27] Ch. Jung, M. Lücke, and P. Büchel, Phys. Rev. E **54**, 1510 (1996). JLB scale temperatures by $\kappa\nu/(\alpha g d^3)$ and concentration by $\kappa\nu/(\beta g d^3)$. Thus the relation between the respective reduced fields is $T_{JLB} = \mathrm{Ra}\, T$ and $C_{JLB} = \mathrm{Ra}\, C$.

[28] F. H. Harlow and J. E. Welch, Phys. Fluids **8**, 2183 (1965); J. E. Welch, F. H. Harlow, J. P. Shannon, and B. J. Daly, Los Alamos Scientific Laboratory of the University of California, Report No. LA-3425, 1966 (unpublished); C. W. Hirt, B. D. Nichols, and N. C. Romero, Los Alamos Scientific Laboratory of the University of California, Report No. LA-5852, 1975 (unpublished).

[29] R. Peyret and T. D. Taylor, *Computational Methods in Fluid Flow* (Springer-Verlag, Berlin, 1983).

[30] J. Niederländer, M. Lücke, and M. Kamps, Z. Phys. B: Condens. Matter **82**, 135 (1991).

[31] W. Barten, M. Lücke, W. Hort, and M. Kamps, Phys. Rev. Lett. **63**, 376 (1989).

[32] S. Chandrasekhar, *Hydrodynamic and Hydromagnetic Stability* (Dover Publications, New York, 1981).

[33] S. Hollinger, P. Büchel, and M. Lücke, Phys. Rev. Lett. **78**, 235 (1997).

[34] H. B. Squire, Proc. R. Soc. London, Ser. A **142**, 621 (1933).

[35] E. Knobloch and D. R. Moore, Phys. Rev. A **37**, 860 (1988).

[36] M. C. Cross and K. Kim, Phys. Rev. A **37**, 3909 (1988).

[37] W. Schöpf and W. Zimmermann, Phys. Rev. E **47**, 1739 (1993).

[38] W. Hort, Diplom thesis, Universität des Saarlandes, Saarbrücken, 1990.

[39] G. W. T. Lee, P. Lucas, and A. Tyler, J. Fluid Mech. **135**, 235 (1983).

[40] S. Hollinger and M. Lücke, Phys. Rev. E **52**, 642 (1995).

[41] S. J. Linz and M. Lücke, Phys. Rev. A **35**, 3997 (1987); **36**, 2486(E) (1987).

[42] D. T. J. Hurle and E. Jakeman, J. Fluid Mech. **47**, 667 (1971).

[43] P. Kolodner, C. M. Surko, and H. L. Williams, Physica D **37**, 319 (1989).

[44] T. Clune and E. Knobloch, Physica D **61**, 106 (1992).

[45] S. J. Linz and M. Lücke, in *Propagation in Systems Far from Equilibrium*, edited by J. E. Wesfreid, H. R. Brand, P. Manneville, G. Albinet, and N. Boccara (Springer-Verlag, Berlin, 1988), p. 292.

[46] M. C. Cross and K. Kim, Phys. Rev. A **38**, 529 (1988).

[47] H. W. Müller, M. Lücke, and M. Kamps, Phys. Rev. A **45**, 3714 (1992).

[48] Ch. Jung, Diploma thesis, Universität des Saarlandes, Saarbrücken, 1993.

[49] W. Barten, Ph.D. thesis, Universität des Saarlandes, Saarbrücken, 1992; *Stationäre Konvektion, Ausgedehnte und Lokalisierte Wandernde Konvektionswellen in Zweikomponentigen Flüssigkeiten* (Dengmerter Heimatverlag, St. Ingebert, 1993).

[50] R. W. Walden, P. Kolodner, A. Passner, and C. M. Surko, Phys. Rev. Lett. **55**, 496 (1985).

[51] R. Heinrichs, G. Ahlers, and D. S. Cannell, Phys. Rev. A **35**, 2761 (1987).

[52] J. Fineberg, E. Moses, and V. Steinberg, Phys. Rev. A **38**, 4939 (1988).

[53] V. Steinberg, J. Fineberg, E. Moses, and I. Rehberg, Physica D **37**, 359 (1989).

[54] S. Hollinger, M. Lücke, and H. W. Müller, Phys. Rev. E **57**, 4250 (1998).

[55] S. Fauve, S. Douady, and O. Thual, J. Phys. (France) **50**, 311 (1989).

[56] H. Schmitt, Diplomarbeit, Universität des Saarlandes, Saarbrücken, 1992.

[57] C. Fütterer, Ph.D. thesis, Universität des Saarlandes, Saarbrücken,1998.

[58] D. Bensimon, P. Kolodner, C. M. Surko, H. L. Williams, and V. Croquette, J. Fluid Mech. **217**, 441 (1990).

[59] P. Kolodner, D. Bensimon, and C. M. Surko, Phys. Rev. Lett. **60**, 1723 (1988).

[60] B. L. Winkler and P. Kolodner, J. Fluid Mech. **240**, 31 (1992).